 doi:10.20944/preprints202203.0142.v1

Article

The Ulug-Sair Gold-Bismuth Ore Occurrence (Western Tuva, Russia): PT Parameters, The Composition of Fluids, and Isotopy of S and O

Renat V. Kuzhuget[1,*], Natalia N. Ankusheva[2,3]*, Andrey A. Mongush[1], Yuri V. Butanaev[1] and Nadezhda V. Suge-Maadyr[1]

[1] Tuvinian Institute for Exploration of Natural Resources of Siberian Branch of RAS (TuvIENR SB RAS), Republic of Tyva, 667007 Kyzyl, Russia; rkuzhuget@mail.ru (R.V.K); kadyrool91@mail.ru (Ch.O.K); amongush@inbox.ru (A. A.M); jyra3@mail.ru (Yu.V.B);

[2] South Urals Federal Research Center of Mineralogy and Geoecology UB RAS, Institute of Mineralogy, Chelyabinsk district, 456317 Miass, Russia; ankusheva@mail.ru (N.N.A);

[3] South Urals State University, Chelyabinsk district, 456314 Miass, Russia;

* Correspondence: ankusheva@mail.ru (N.N.A); rkuzhuget@mail.ru (R.V.K)

Abstract: We examined PT parameters, geochemical peculiarities, and fluid sources of the Ulug-Sair ore occurrence attributable to class of intrusion-related gold deposits and according to ore mineral assemblages corresponding to Au-Bi type with wide Bi minerals (AgBiTe, Bi_2Te_2Se, $Cu_{3,07}BiS_3$, Bi), tellurides (Au and Ag), Se-tellurides (Ag and Bi), and selenides (Au, Ag, and Hg). We identified that 'pre-gold' quartz-tourmaline veins were deposited using an aqueous Mg-Na-K-chloride fluid with a salinity of 8–10 wt % NaCl eq. At 325–370 °C; host breasts were formed due to a CO_2-water fluid containing CH_4 and N_2, with a salinity of 0,18–6,1 wt % NaCl eq. at least 200–400 °C. Gold-bearing mineral assemblages were formed at P ~ 0,75–1,0 kbar (~ 2,3–3 km) due to CO_2-water chloride (Na-K±Fe, Mg) fluid with CH_4, Na_2SO_4, and $Na_2B_2O_5$, and salinities 1,7–12,5 wt % NaCl eq. during the decreasing temperatures from 360 up to 115 °C (gold-sulfide-quartz veins – 360–130 °C, and gold-telluride-sulfide-quartz veins – 330–115 °C) and variations fO_2, fS_2, fSe_2, and fTe_2. The isotopic composition of $\delta^{34}S_{H_2S}$ fluid (-0,7…+2,5 ‰) indicates the juvenile or magmatic origin of fluid and ore elements. The $\delta^{34}O_{H_2O}$ fluid indicates that, at an early substage, the formation of ore occurrence involved a fluid of magmatic or metamorphic origin (+7,3…+11,4 ‰), and, in the later substage, it mixed with meteoric waters (-2,3…+9,1 ‰).

Keywords: gold; fluid inclusions; quartz; stable isotopes; gold deposits, Western Tuva

1. Introduction

During the geological survey, searching, and prospecting work of 1952–1977 in Western Tuva, gold-quartz ore occurrences were discovered (Ulug-Sair, Aryskan, Khaak-Sair, Dushkunnug, Ak-Dag, etc.) and numerous gold mineralization points associated with medium-temperature beresite and listvenite metasomatites. The largest of them are the occurrences of the Khaak-Sair in listvenites [1] and the Ulug-Sair – in conglomerates, siltstones, and beresites. They are located in the Aldan-Maadyr ore cluster (AMOC), which is considered one of the promising ore clusters for native Au (Figure 1) in the region.

Preprints (www.preprints.org) | NOT PEER-REVIEWED | Posted: 10 March 2022 doi:10.20944/preprints202203.0142.v1

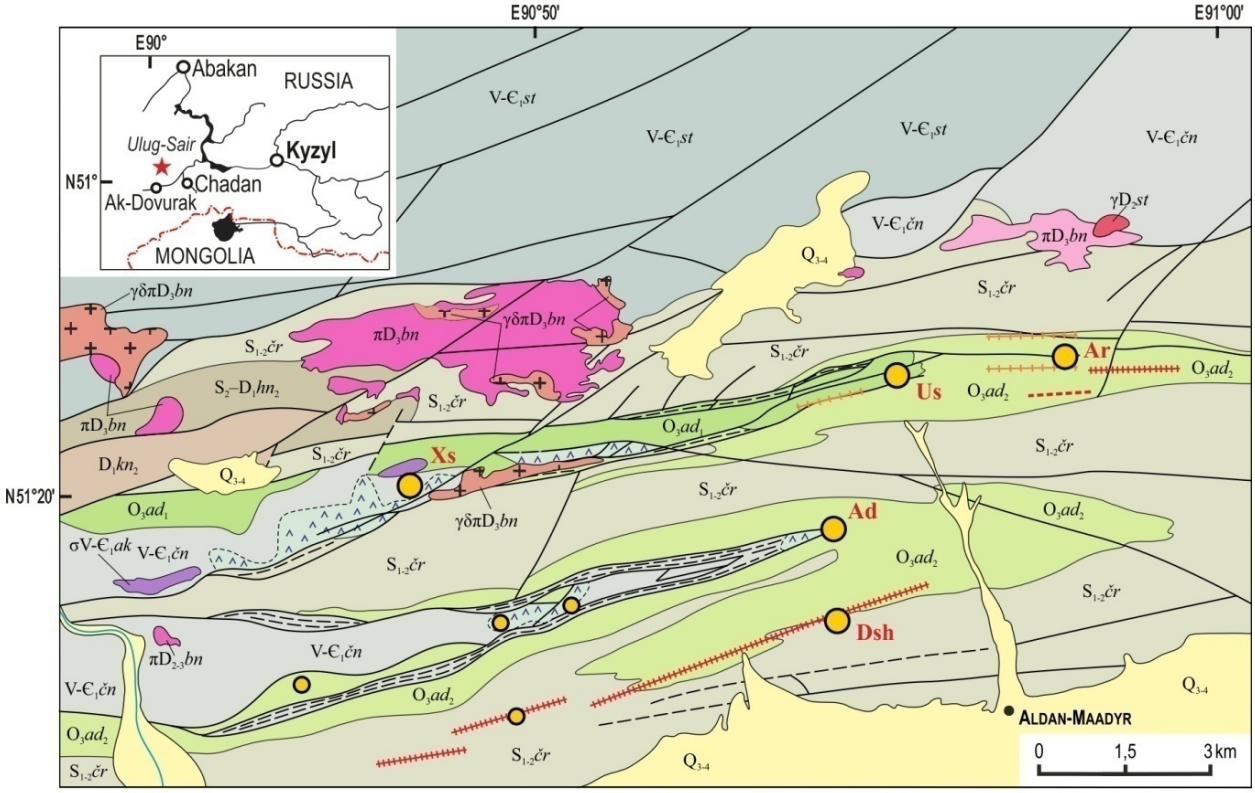

Q3-4 Alluvial and deluvial sediments (Q3-4)

D1kn2 Rhyolites of the Upper Candacean Formation (D1kn2)

S2–D1hn2 Red-colored sandstones and siltstones of the Upper Hondergean Formation (D1hn2)

S1-2čr Sericite-clayey shales of the Cherkasy Formation (S1čr)

O3ad2 Siltstones with interlayers of sandstone of the Upper Adyrtash Formation (O3ad2)

O3ad1 Shale conglomerates, siltstones and sandstones of the Lower Adyrtash Formation (O3ad1)

V-Є1st Sericite-chlorite quartz shales, metamorphosed silts of the Syutkhol Formation (V-Є1st)

V-Є1čn Effusives, tuffs, serpentinites, siltstones, sandstones and shales of the Chingin Formation (V-Є1čn)

γD2st Granites of Syutkhol complex (D2st)

Intrusive rocks of Bayankol complex (D3bn)

Diorites of III phase

γδπD3bn Quartz, andesite and rhyolite porphyries of II phase

+ πD3bn Granodiorite, tonalite and granite porphyries, rhyolites of I phase

σV-Є1ak Serpentinites, peridotites, pyroxenites, and associated gabbroids and diorites of the Akdovrak ophiolite complex (σV-Є1ak)

Listwanite

Dykes of beresitized rhyolites of II phase of the Bayankol complex (D3bn)

Beresites by Ordovician sedimentary rocks

a Geological (a) and facial (b) boundaries
b

a Faults: reliable (a) and assumed (b)
b

Tectonic zones

Gold mineralization

Gold ore occurences

Ad Gold ore occurrence (Khs – Khaak-Sair, Us – Ulug-Sair, Ar – Aryskan, Ak – Ak-Dash, Ad – Ak-Dag, Dsh – Dushkunnug)

Figure 1. Geological scheme of the central part of AMOC (according to E.V. Zaykova and V.V. Zaykov [2], modified).

AMOC is located on the left bank of the Khemchik River and confined to the junction zone: a) Early Cambrian-Ordovician terrigenous complexes of the Western Sayany; b) Vendian-Early Cambrian oceanic chaotic complexes and Middle Cambrian-Silurian molasses, which, respectively, formed the foundation and sedimentary cover of the Khemchik-Systygkhem pre-arc collision deflection; and c) Devonian magmatic and sedimentary complexes of one of the "branches" of the Tuva riftogenic trough [3,4].

Gold mineralization is controlled by narrow linear anticlines and horst anticlines of a sub-latitudinal strike and the supporting fractures of the Sayany-Tuva deep fault of the same orientation cutting them. A similar orientation of the main discontinuous and

Preprints (www.preprints.org) | NOT PEER-REVIEWED | Posted: 10 March 2022 doi:10.20944/preprints202203.0142.v1

folded structures led to a linear distribution of igneous rocks and narrow linear zones of metasomatites of the beresites & listvenite series with gold-quartz veins.

Gold mineralization is associated with intrusions of the Bayankol complex (D3bn) which are represented as dikes of as follows granodiorite- and tonalite porphyry, rhyolite and granodiorite porphyry dykes [5].

Gold mineralization is paragenetically related to the intrusions of the Bayankol complex (D3bn), which are represented as dikes of granodiorite and tonalite porphyries, rhyolites, and granodiorite porphyries [5]. The results of $^{40}Ar/^{39}Ar$ dating of synore listvenites (379.4 ± 4.4 Ma) of the Khaak-Sair ore occurrence are agreed very well with the $^{40}Ar/^{39}Ar$ age (376.5 ± 3.4 Ma) of phase III gabbro dikes of the Bayankol intrusive complex (D_3bn), confirmed the genetic relationship of mineralization with the Late Devonian Bayankol intrusive complex [6,7].

AMOC is one of the perspective ore clusters for native Au in the region. Ore occurrences of AMOC are characterized by the low sulfide content (< 3 %) and by the presence of the Au-Bi-Te-Se mineral assemblages namely petzite, hessite, altaite, coloradoite, Te-bismuthite, tsumoite, Se-volynskite, kawazulite, wittichenite, native Bi, fischesserite, clausthalite, naumannite, and tiemannite [7,8].

The relevance of the study is to determine the mineralogical-geochemical features and fluid regime of the Ulug-Sair gold-quartz ore occurrence with a peculiar mineral composition of the ores characterized by the presence of tellurides (Ag_3AuTe_2, Ag_2Te), selenides (Ag_3AuSe_2, Ag_2Se, HgSe) and diverse Bi minerals (AgBiTe, Bi_2Te_2Se, $Cu_{3,07}BiS_3$, Bi).

2. Geological setting

The Ulug-Sair ore occurrence is located in the central part of AMOC and was discovered in 1964 by Victor V. Zaykov during the geological survey in 1:50000 scales [2]. It is confined to the axial part of the host-anticline of sub-latitudinal strike and complicated by feathering faults: in the north – Arzhansky Fault, in the south – "Ore" Fault accompanied with numerous cracks with incidence angles of 75–90°. The core of the horst anticline is composed of Ordovician conglomerates, siltstones, sandstones, and Vendian-Lower Cambrian ophiolites (exposed west of the ore occurrence), the wings are composed of Ordovician siltstones, Silurian schists, and siltstones (Figure 1).

The Ulug-Sair horst anticline is 6 km long and the wingspan is 2–3 km. Lilac-gray small-pebble schist conglomerates of the Ordovician (O_3ad_1) Lower Adyrtash subsuites, which lies in the core of the Ulug-Sair horst anticline, are wrinkled into small folds and contain a large amount of gold-quartz veins. Pebbles in conglomerates with silt cement are represented by semi-rounded, sometimes angular vein quartz and quartzite from 1 to 5 cm. It makes up 50–60 % of the rock bulk. Conglomerates contain interlayers of greenish-gray schist sandstones of 10 to 25 m thick and gravelites of 0.2–1.5 m thick. The conglomerates, by and with a gradual transition, are overlapped with lilac and gray-green siltstones of the Upper Adyrtash sub formation (O_3ad_2). Siltstones contain greenish-gray, lilac-gray, and red-brown sandstones in the form of interlayers of 0.01 to 5 m thick, as well as packs with a thickness of several tens of meters. The total thickness of the rocks of the Upper Adyrtash Formation is 600–700 m.

The rocks of the Silurian Nizhny Chergak sub formation ($S_1čr_1$) are concordantly overlapped with the rocks of the Upper Adyrtash sub formation (O_3ad_2) and represented by gray, greenish-gray sericite-clay shales with gray-green aleurolites and gray sandstones of 68–140 m and 1.5–20 m thick, respectively.

Igneous rocks are represented by dykes, rhyolite-, granodiorite-porphyries (II phase), and diorites (III phase) of the Bayankol complex (D_3 bn) in the Ordovician and Silurian rocks. he fall of dykes is vertical; contacts with host rocks are transversal. Dykes of light gray rhyolite-porphyry are confined to the western flank of the ore occurrence, and gray-green granodiorite-porphyry – to its northern flank. The dykes of greenish-gray diorites are the most widespread.

Preprints (www.preprints.org) | NOT PEER-REVIEWED | Posted: 10 March 2022 doi:10.20944/preprints202203.0142.v1

At the Ulug-Sair, quartz-tourmaline metasomatites, beresites after intrusive and sedimentary rocks, as well as quartz veins and vein zones with gold mineralization are formed (Figure 2). More than 75 gold-quartz veins and several vein zones of the EW strike with a dip close to vertical were identified. The veins are from 15 cm to 2 m thick, and 20–100 m long (less often 200 m); vein zones are 3 to 40 m thick and 20 to 120 m long [2]. The average content of ore minerals in ores does not exceed 3 %.

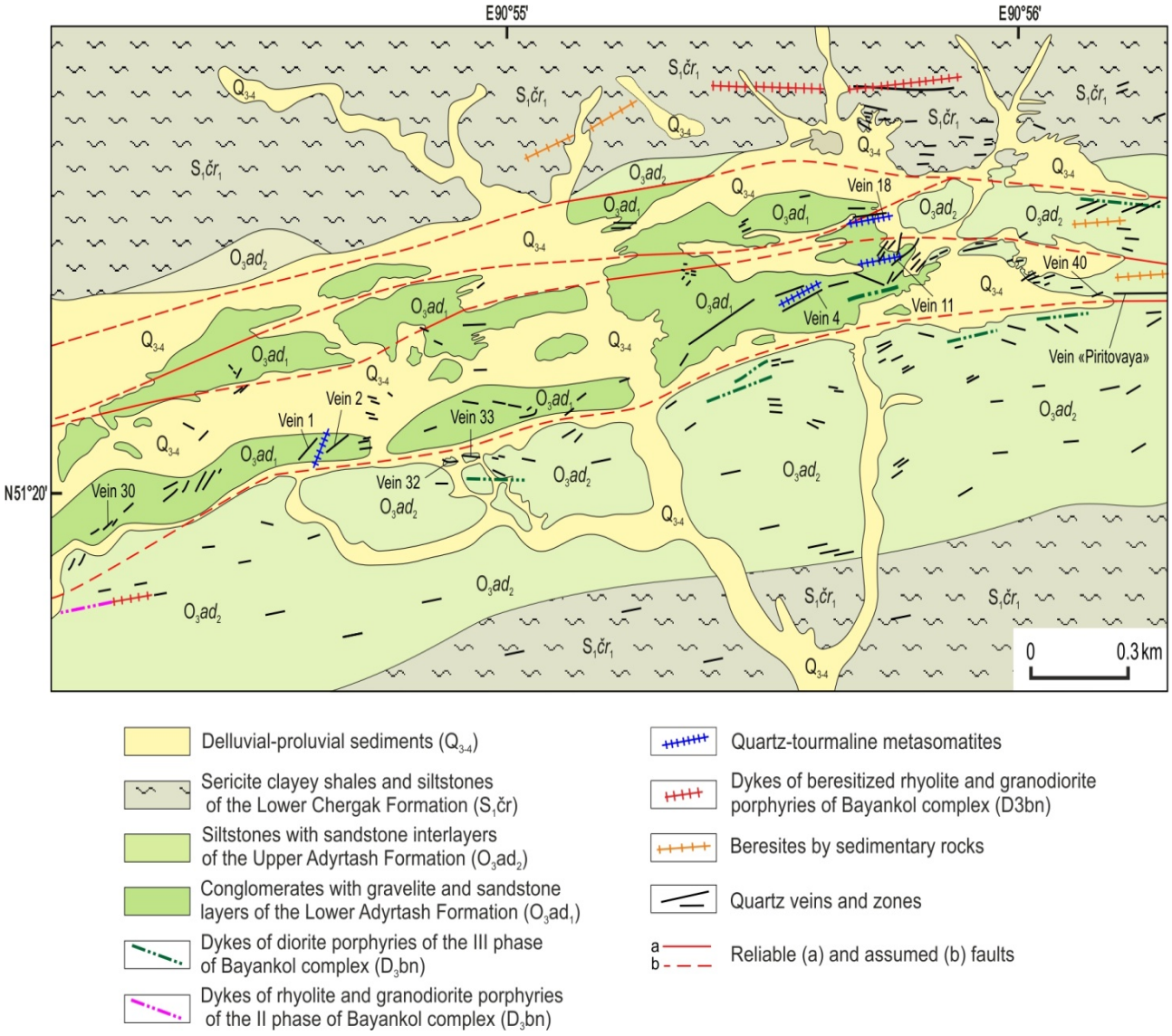

Figure 2. Geological scheme of the Ulug-Sair ore occurrence (according to E.V. Zaykova, V.V. Zaykov [2], modified).

The Au content in quartz veins ranges from 0.2 to 286 ppm; and Ag – from traces up to 300 ppm [2]. The Au resources of the P_2 category, according to the prospecting work of 'Krasnoyarskgeolsjemka' OJSC, are 20 t with average Au content of 2 ppm [9]. The Cu sulfides in quartz veins marked their gold enrichment. In ores, a positive correlation between Au and Cu, B, Ag, Sb, As, Te, Bi, Mn, Ba, Sr, Pb, Mg, Mo, Cd, Zn, and W was identified [10].

2. Materials and Methods

The optical studies were carried out using Olympus BX41, POLAM P-213M, and P-212M microscopes (TuvIENR SB RAS, Kyzyl). The chemical composition of minerals was determined using a MIRA 3 LMU SEM (Tescan Orsay Holding) with INCA Energy

 doi:10.20944/preprints202203.0142.v1

450 + XMax 80 and INCA Wave 500 microanalysis systems (Oxford Instruments Nanoanalysis Ltd) (Institute of Geology and Mineralogy SB RAS, Novosibirsk). We used the ontogenic peculiarities (composition, structure, zoning, and induction surfaces) to examine the sequence of mineral formation in ores, including the intersections of early mineral aggregates with the latest ones, as well as the presence of previously formed fragments in late mineral aggregates.

The Au and Au-Ag minerals (cubic solid solutions) are described using the terminology from [11,12]: native gold (1000–700‰: ultrahigh-fineness (1000–950‰), high-fineness (950–900‰), medium-fineness (900–800‰), and low-fineness (800–700‰)), electrum (700–300‰), kustelite (300–100‰), and Au-bearing silver with a fineness of <100‰.

The fluid inclusion study was carried out in the thermobarogeochemistry laboratory of the South Urals State University (Miass) and the CCE "Multielement and Isotope Studies" SB RAS (Novosibirsk) using the Linkam TMS-600 stage equipped with LinkSystem 32 DV-NC and optical Olympus BX51 microscope. The eutectic temperatures of fluid inclusions are interpreted using [13,14]. The salinity of inclusions was determined by the final melting temperatures according to [15]. The homogenization temperatures are the first temperature of the process of mineral formation [16]. The results were processed in Statistica 12.

PT for mineral assemblages is also determined using geothermometers, geofugometers, and mineral parageneses. The stability areas of the main ore minerals in the $fS_2 - fTe_2$ и $fS_2 - fSe_2$ coordinates are examined from [17–20].

The gas composition of fluid inclusions was detected by Raman spectroscopy on a Ramanor U-1000 spectrometer with a Horiba DU420E-OE-323 detector (Jobin Yvon) and a Millennia Pro laser from Spectra-Physics (analyst A.A. Redina, Institute of Geology and Mineralogy SB RAS, Novosibirsk). The pressure of fluid inclusions was calculated using the FLINCOR program using CO_2 homogenization temperatures [21].

The bulk analysis of the element composition of fluid was carried out according to [22]. The gases from inclusions (H_2O, CO_2, and CH_4) were analyzed by an Agilent 6890 gas chromatograph. The content of anions in the aqueous extract was determined by ion chromatography (Color-3000); the cations and trace elements – by the ICP MS analysis (Elan-6100). The NSO_3 content was calculated on the balance sheet. To exclude the influence of the matrix, a repeated ("single") extraction was carried out, the analysis of which was subtracted from the first one.

The oxygen isotopic composition was analyzed on Isoprime mass spectrometer using the internal AQS standard (Akita Quartz Standard) at the University of Akita, Japan (analysts H. Kawaraya and O. Matsubaya). The values of $\delta^{18}O$ are in ppm (‰) relative to the SMOW standard.

The isotopic composition of sulfur in sulfides was analyzed at the Multi-element and Isotope Research Center SB RAS using a Finnigan MAT Delta gas mass spectrometer in dual-inlet mode (analysts V.N. Reutsky and M.N. Kolbasova, Novosibirsk). The measurement control was provided by the samples with standard isotopic composition in the range $\delta^{34}S$ from -15.1 to + 21.8 ‰ relative to troilite from Canyon Diablo (CDT), including international ones: NBS-123 ($\delta^{34}S$ = +17.44) and NBS-127 ($\delta^{34}S$ = +21.8). The reproducibility of the values of $\delta^{34}S$, including sample preparation, is not more than 0.1 ‰ (2σ). The values of $\delta^{34}S$ (‰) are given relative to the CDT standard.

3. Results

3.1. Mineral composition of ores

Pre-ore quartz-tourmaline metasomatites are replaced by the gold-sulfide-quartz mineralization in beresites within the Ulug-Sair ore occurence. We identified based on the previous works [2] and our data that the earliest high-temperature quartz-tourmaline

Preprints (www.preprints.org) | NOT PEER-REVIEWED | Posted: 10 March 2022 doi:10.20944/preprints202203.0142.v1

stage includes two substages: tourmaline and tourmaline-quartz. Gold-sulfide-quartz mineralization includes 7 substages: pre-ore beresite and pyrite-quartz; ore gold-sulfide-quartz (I) and gold-telluride-sulfide-quartz (II); and post-ore chlorite-quartz, carbonate-quartz, and chlorite-hematite-quartz substages. Limonite, malachite, azurite, goethite, scorodite, cuprite, cerussite, bismutite, iodargyrite, and chlorargyrite are secondary and formed in the weathering crust (Figure 3).

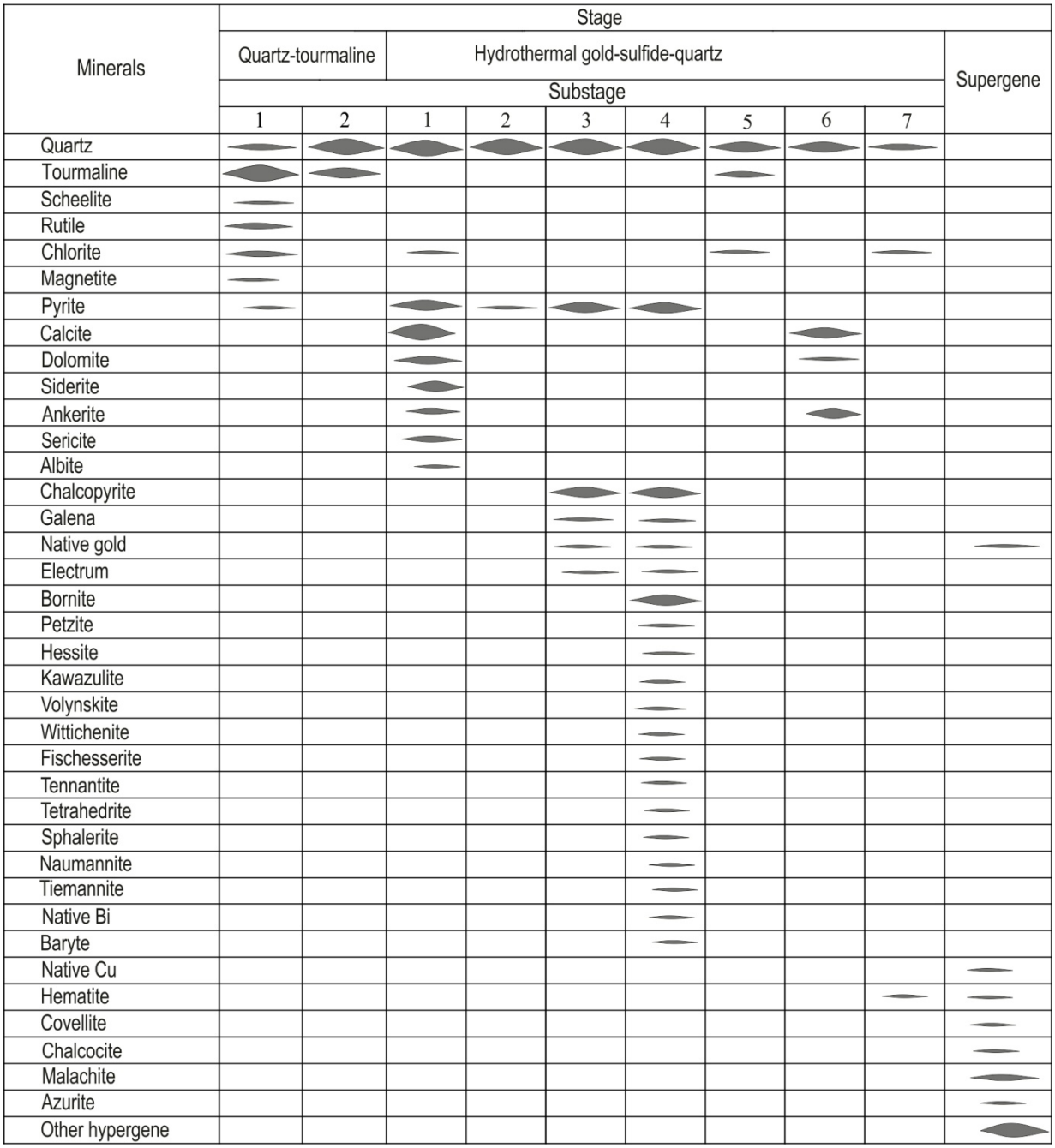

Figure 3. The sequence of mineral formation at the Ulug-Sair ore occurrence.

Quartz-tourmaline metasomatites and veins are widespread throughout the entire ore occurrence (Figure 4a–b). They contain rutile (including W-containing), F-apatite, scheelite, and pyrite. They are metasomatic rocks formed after Ordovician aleurolites and

Preprints (www.preprints.org) | NOT PEER-REVIEWED | Posted: 10 March 2022 doi:10.20944/preprints202203.0142.v1

conglomerates up to 5–7 m thick and composed of light green needle-prismatic tourmaline.

Figure 4. Metasomatites of the Ulug-Sair ore occurrence: (a) quartz-tourmaline metasomatites (1) with tourmaline-quartz (2) and gold-sulfide-quartz (3) veins of the latest substages; b) brecciated fragments of quartz-tourmaline metasomatites (1) in gold-sulfide-quartz mineral aggregates (3); (c–d) ore-bearing conglomerates (1) with tourmaline-quartz (2) and sulfide-quartz (3) veins; (e–f) beresite with gold-sulfide-quartz veins after c) rhyolite porphyry (3); d) quartz sandstone (3).

The chemical composition of tourmaline from quartz-tourmaline metasomatites and veins shows that they are related to the intermediate members of the dravite-magnesio-foitite series, where the magnesio-foitite component predominates (X_{Fe} 0.80–1.38 cf.). The content of Fe^{3+} 0.00–0.15 cf.; Fe^{3+}/Fe_{total} = 0.00–0.11; Fe^{2+} and Fe^{3+} are

Preprints (www.preprints.org) | NOT PEER-REVIEWED | Posted: 10 March 2022 doi:10.20944/preprints202203.0142.v1

calculated from the charge balance. The X_{Fe} increases from early to latest one (from 0.80–0.91 up to 0.92–1.28 cf). Also, an isomorphism of Mg,(Al) → Fe is in tourmaline. The ratio Fe^{3+}/Fe_{total} is low and ranged between 0.00 and 0.08 [10].

Two types of beresites formed after intrusive and sedimentary rocks, respectively, were formed (Figure 4c–d). In both cases, hydrothermal-metasomatic alteration is presented by silicification, sericitization, pyritization, and carbonatization of rocks. The relics of primary rocks are often in beresites: on the first way, rhyolite and granodiorite porphyries, in the second, sandstones, siltstones, and conglomerates. The alterations from beresites to them are gradual. The mineral composition of the beresites of both types is similar – yellow hydrothermally altered, fine and cryptocrystalline rocks with thin pyrite-quartz and carbonate veins, composed of quartz (30–50 %), albite (40–60 %), sericite (up to 5–10 %), calcite, ankerite (up to 10–30 %) and pyrite in the form of well-faceted cubic crystals (1–15 %) with an average size of 1–5 mm, reaching a maximum of 1–3 cm.

The dykes of rhyolite and granodiorite porphyries are intensely beresitized; in diorite dykes; beresitization is insignificant in the form of thin zones (up to 5 cm) in the selvages of thin gold-sulfide-quartz veins. The strike of dykes is sublatitudinal and consistent with the directions of the faults. They have clear contacts, a vertical or close drop to them. The shape of the dykes is plate-like, slightly curved, and sometimes vein-like; 1–3 m thick and 0.3–0.5 km long, less often up to 1 km.

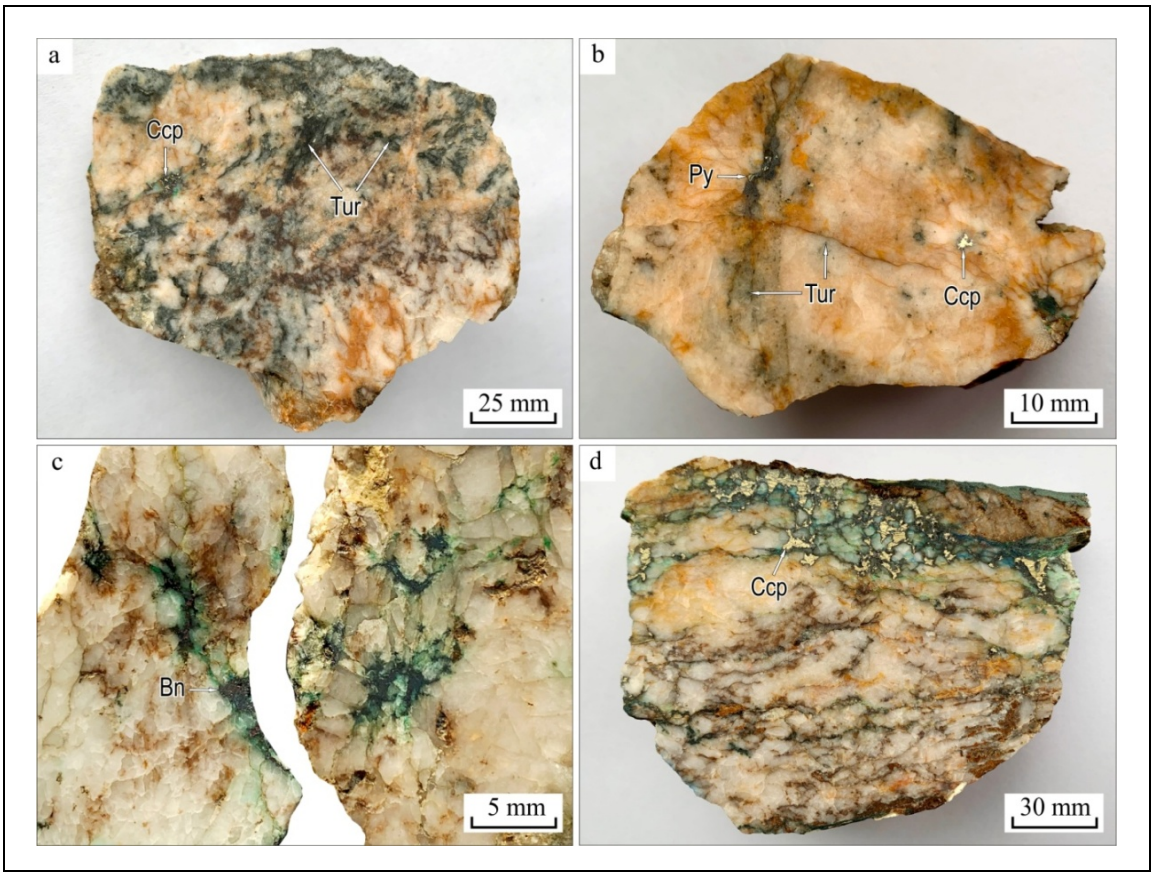

Figure 5. Ore textures of the Ulug-Sair ore occurrence: (a–b) vein-disseminated gold-sulfide-quartz ores with chalcopyrite (Csp), pyrite (Py) and early brecciated tourmaline (Tur); (c–d) vein-disseminated gold-telluride-sulfide-quartz ores with bornite (Bn) and chalcopyrite (Ccp).

Beresites after sandstones, aleurolites, and conglomerates have a "splinous", like a "ponytail" body shape and steep (with angles of incidence of 75–85°), sometimes vertical bedding by the host rocks. They vary in thickness from 0.5 to 2 m and a length of 100 to

 doi:10.20944/preprints202203.0142.v1

150 m. The rhyolite and granodiorite porphyry dykes are hypsometrically lower than the beresitized sedimentary rocks in the beresitized zones along the sedimentary rocks.

Later, gold-sulfide-quartz and gold-telluride-sulfide-quartz veins are formed overlaid quartz-tourmaline metasomatites and beresites and beresitized rocks (Figure 5).

Gold-sulfide-quartz veins (I) are widespread and formed vein zones composed of quartz, chalcopyrite, pyrite, galena, gold, and electrum. The main ore mineral – chalcopyrite – formed phenocrysts and 'nests' in quartz. Pyrite is formed cubic and pentagon-dodecahedral crystals. Two mineral assemblages are formed in the gold-sulfide-quartz veins: early gold-galena-pyrite-chalcopyrite-quartz and the latest gold-electrum-pyrite-chalcopyrite-quartz. Their formation is accompanied by deformations of tourmaline metasomatites and followed by brecciation of tourmaline in quartz veins in the form of tourmaline xenoliths or radially radiant aggregates (up to 5 % of the vein) (Figure 5).

Gold in gold-sulfide-quartz veins (I) of lumpy, interstitial, elongated, crystallomorphic (octahedra, cuboctahedra, crystal intergrowths, and weakly faceted aggregates) and dendritic shapes is disseminated in quartz and chalcopyrite, in intergrowth with pyrite and brecciated tourmaline (Figure 6). Electrum of lumpy-branched and interstitial shapes is detected in intergrowths with chalcopyrite in quartz; and rare.

The chemical composition of gold is (wt %) Au 72.12–96.44, Ag 3.36–27.69, Cu 0.00–0.69, Te 0.00–0.04; electrum – Ag 29.80–38.45, Au 61.55–69.71, Cu 0.00–0.46. Gold and electrum grains are weakly zoned with an increase of Ag amount to the grain periphery by 3–7 wt %.

Gold-telluride-sulfide-quartz veins (II) with disseminated, nest- and vein-disseminated mineralization are up to 2 m thick and up to 28 m long. Gold (up to 0.3 mm) of interstitial, lumpy-branched, and cementation shapes are accompanied by quartz, chalcocite, hessite, petzite, malachite, and Fe hydroxides. Lumpy and lumpy-branched electrum is found in quartz and Fe hydroxides. Gold and electrum are associated with chalcopyrite, bornite, galena (Se up to 0.64 wt %), tennantite, tetrahedrite, sphalerite, kawazulite, fischesserite, naumannite, tiemannite, Se-volynskite, wittichenite, native Bi, and Cu.

The chemical composition of this gold is (wt %) Au 72.56–90.10, Ag 9.47–27.44, Cu 0.00–0.50, and Te 0.00–0.02; electrum – Au 60.37–69.45 and Ag 30.53–40.12. In gold, the Au amount from the center to the edge of the grains is decreased by 2–5 wt % with increasing of Ag.

Small inclusions (1–50 μm) of hessite and petzite are detected in chalcocite; less often bornite and quartz (Figure 7).

Preprints (www.preprints.org) | NOT PEER-REVIEWED | Posted: 10 March 2022 doi:10.20944/preprints202203.0142.v1

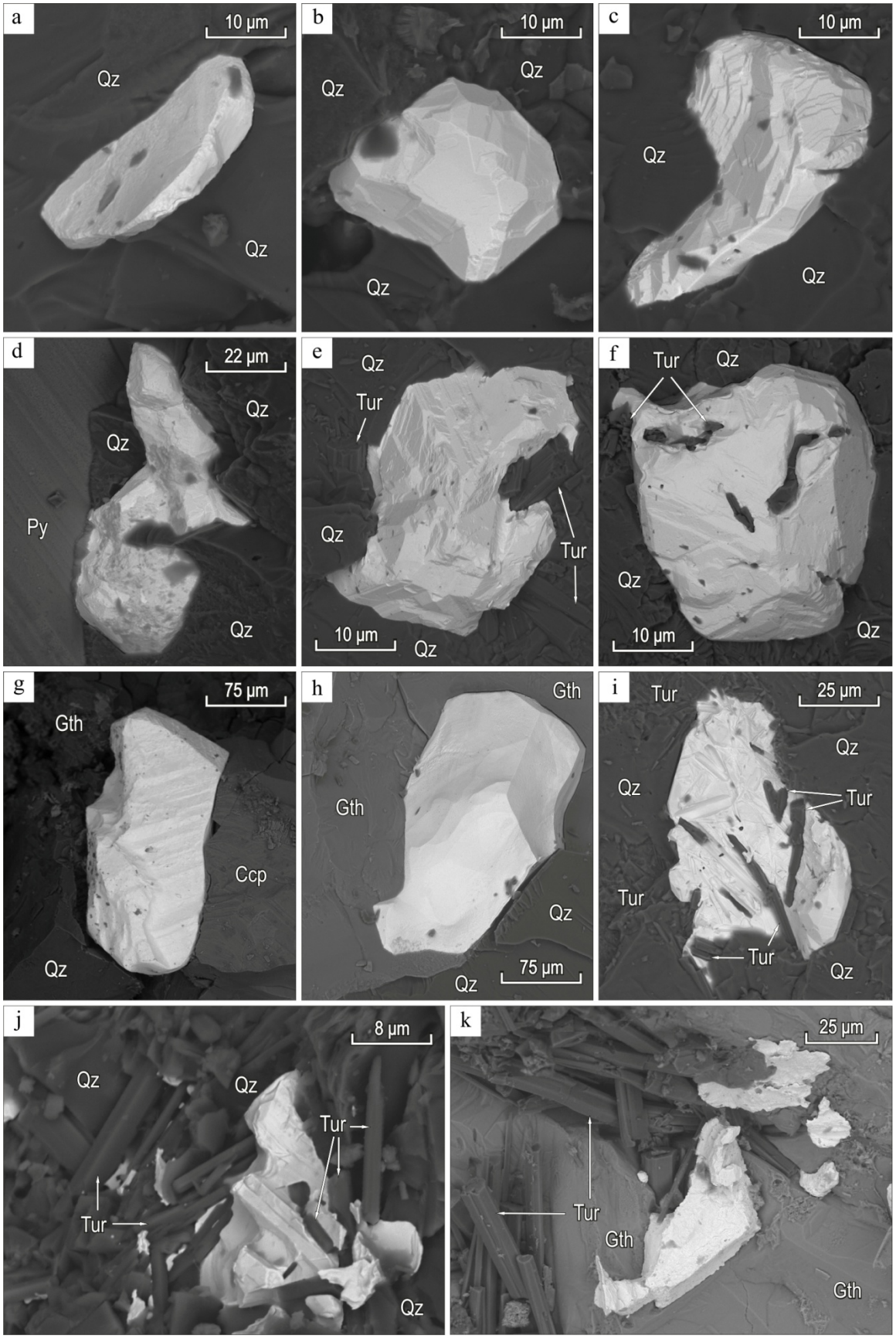

Figure 6. Gold (light) in gold-sulfide-quartz veins with pyrite, chalcopyrite, and goethite (Gth), and early tourmaline (Tur) from quartz-tourmaline metasomatites. BSE photos.

Preprints (www.preprints.org) | NOT PEER-REVIEWED | Posted: 10 March 2022 doi:10.20944/preprints202203.0142.v1

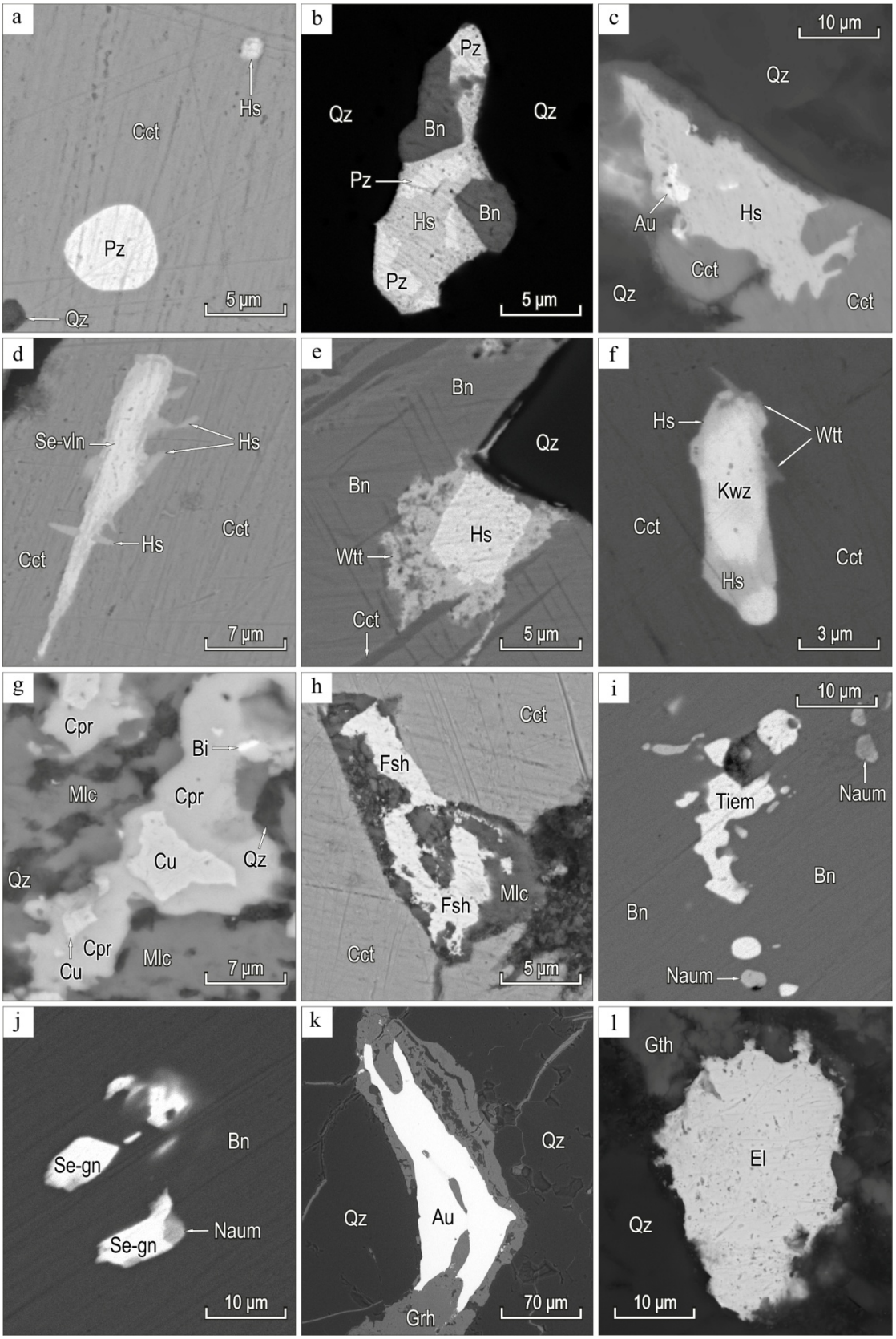

Figure 7. Hessite (Hs), petzite (Pz), Se-volynskite (Vln), wittichenite (Witt), kawazulite (Kwz), native Bi, fischesserite (Fsch), naumannite (Naum), tiemannite (Tiem), Se-galena (Se-gn), gold (Au) and electrum (El) in quartz (Qz), bornite (Bn), chalcocite (Cct) with malachite (Mlc), cuprite (Cpr), native copper (Cu) and goethite (Gth) gold-telluride-sulfide-quartz veins. BSE photos.

Preprints (www.preprints.org) | NOT PEER-REVIEWED | Posted: 10 March 2022 doi:10.20944/preprints202203.0142.v1

Hessite formed the intergrowths with petzite, wittichenite, kawazulite, and Se-volynskite, sometimes up to 4 μm thick in the rims. Petzite in intergrowths with hessite often has round and oval shapes. The compositions of Au and Ag tellurides are stoichiometric (Table 1).

Table 1. Chemical composition of petzite, hessite, fischesserite, naumannite, tiemannite, Se-volynskite, kawazulite, and wittichenite, wt %.

№	Au	Ag	Bi	Cu	Hg	Pb	Te	Se	S	Total	Crystallochemical formula
						Petzite					
1	25.21	41.56	–	–	–	–	32.69	–	–	99.46	$Ag_{3.00}Au_{1.00}Te_{2.00}$
2	25.10	41.55	–	–	–	–	33.15	–	–	99.80	$Ag_{2.99}Au_{0.99}Te_{2.02}$
						Hessite					
3	–	63.12	–	–	–	–	36.47	–	–	99.59	$Ag_{2.02}Te_{0.98}$
4	–	62.22	–	–	–	–	37.29	–	–	99.51	$Ag_{1.99}Te_{1.01}$
5	–	62.29	–	–	–	–	37.47	–	–	99.76	$Ag_{1.99}Te_{1.01}$
6	–	62.08	–	–	–	–	37.34	–	–	99.42	$Ag_{1.99}Te_{1.01}$
7	–	62.38	–	–	–	–	36.86	–	–	99.24	$Ag_{2.00}Te_{1.00}$
8	–	62.25	–	–	–	–	37.55	–	–	99.80	$Ag_{1.99}Te_{1.01}$
9	–	61.85	–	–	–	–	37.37	–	–	99.22	$Ag_{1.99}Te_{1.01}$
10	–	62.64	–	–	–	–	36.76	–	–	99.40	$Ag_{2.01}Te_{0.99}$
						Fischesserite					
11	27.95	48.70	–	–	–	–	–	23.07	–	99.72	$Au_{0.96}Ag_{3.06}Se_{1.98}$
12	27.39	48.86	–	–	–	–	–	23.27	–	99.52	$Au_{0.94}Ag_{3.06}Se_{2.00}$
13	26.12	49.16	–	–	–	0.70	0.32	23.36	–	99.66	$(Au_{0.89}Pb_{0.03})_{0.91}Ag_{3.07}(Se_{1.99}Te_{0.02})_{2.01}$
14	26.74	48.60	–	–	–	0.98	0.62	22.57	–	99.51	$(Au_{0.92}Pb_{0.03})_{0.95}Ag_{3.07}(Se_{1.95}Te_{0.03})_{1.97}$
						Naumannite					
15	–	72.69	–	–	–	–	–	26.52	–	99.21	$Ag_{2.00}Se_{1.00}$
16	–	74.75	–	–	–	–	–	22.91	1.80	99.46	$Ag_{2.00}(Se_{0.84}S_{0.16})_{1.00}$
						Tiemannite					
17	–	–	–	–	72.58	–	–	26.49	0.76	99.83	$Hg_{1.00}(Se_{0.93}S_{0.07})_{1.00}$
18	–	–	–	–	72.81	–	–	25.60	1.08	99.49	$Hg_{1.01}(Se_{0.90}S_{0.09})_{0.99}$
19	–	–	–	–	73.65	–	–	23.92	1.97	99.54	$Hg_{1.00}(Se_{0.83}S_{0.17})_{1.00}$
20	–	–	–	–	74.05	–	–	26.98	2.65	99.76	$Hg_{0.99}(Se_{0.79}S_{0.22})_{1.01}$
21	–	–	–	–	74.76	–	–	21.69	2.93	99.38	$Hg_{1.01}(Se_{0.74}S_{0.25})_{0.99}$
22	–	–	–	–	76.69	–	–	17.81	4.84	99.34	$Hg_{1.01}(Se_{0.59}S_{0.40})_{0.99}$
						Se-volynskite					
23	–	19.76	39.23	–	–	–	30.58	9.59	–	99.16	$Ag_{1.00}Bi_{1.03}Te_{1.31}Se_{0.66}$
24	–	20.37	39.17	–	–	–	29.48	10.45	–	99.47	$Ag_{1.02}Bi_{1.01}Te_{1.25}Se_{0.72}$
						Kawazulite					
25	–	–	54.22	–	–	–	36.01	8.98	–	99.21	$Bi_{1.98}Te_{2.15}Se_{0.87}$
26	–	–	55.37	–	–	–	36.50	7.79	–	99.66	$Bi_{2.04}Te_{2.20}Se_{0.76}$
27	–	–	55.17	–	–	–	35.56	8.74	–	99.51	$Bi_{2.02}Te_{2.13}Se_{0.85}$
28	–	–	55.26	–	–	–	35.55	8.28	–	99.09	$Bi_{2.04}Te_{2.15}Se_{0.81}$
29	–	–	55.48	–	–	–	35.61	8.78	–	99.87	$Bi_{2.02}Te_{2.13}Se_{0.85}$
						Wittichenite					
30	–	–	39.93	40.09	–	–	–	–	19.70	99.72	$Cu_{3.07}Bi_{0.93}S_{3.00}$
31	–	–	40.89	39.27	–	–	–	–	19.38	99.54	$Cu_{3.05}Bi_{0.97}S_{2.98}$

Note. Mineral compositions were determined on the MIRA LM electron microscope (analyst N.S. Karmanov, IGM SB RAS). A dash is below detection limits. The formulas of petzite and fischesserite are calculated for 6 at., hessite and naumannite – 3 at., tiemannite – 2 at., Se-volynskite are calculated for 4 at., kawazulite – 5 at., wittichenite – 7 at.

Preprints (www.preprints.org) | NOT PEER-REVIEWED | Posted: 10 March 2022 doi:10.20944/preprints202203.0142.v1

We observed the inclusions of fischesserite, naumannite, tiemannite, kawazulite, wittichenite, and Se-volynskite up to 40 μm and fine intergrowths in quartz, bornite, and chalcocite (see Figure 7).

Fischesserite grains up to 20 μm are in chalcocite. Fischesserite contains small admixtures of Pb (up to 0.98 wt %) and Te (up to 0.62 wt %) (Table 1).

Naumannite and tiemannite up to 25 μm are in bornite, sometimes in the view of their fine intergrowths.

Kawazulite and Se-volynskite (Se up to 10.45 wt %) formed elongated 10–40 μm grains of 3–7 μm wide. Kawazulite formed intergrowths with hessite, less often with Se-wittichenite, which as wittichenite, formed rims (up to 2 μm) around kawazulite.

Au with high and medium fineness prevails; electrum is rare (Fig. 8) at the Ulug-Sair ore occurrence. The average gold fineness is 891 ‰ varied from 602 up to 967 ‰, and the average Au fineness of gold-sulfide-quartz veins (I) is 885 ‰ (615–967 ‰), and gold-telluride-sulfide-quartz veins (II) — 797 ‰ (601–904 ‰).

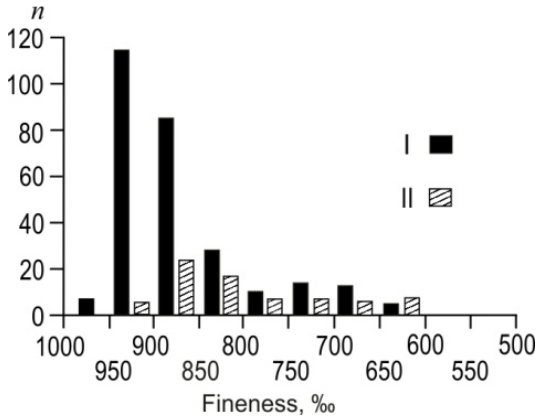

Figure 8. Frequency of native Au fineness of I and II ore substages of the Ulug-Sair ore occurrence.

3.2. Fluid inclusion data of the mineral assemblages

The syngenetic fluid inclusions in quartz of mineral assemblages were analyzed to study the PT parameters of gold-quartz veins from the Ulug-Sair ore occurrence (see Figure 2).

Pseudo-secondary biphase VL fluid inclusions of 10–20 μm in size, oval or isometric shapes with smooth boundaries were studied in quartz of "pre-ore" quartz-tourmaline veins. The eutectic temperatures of the fluid ranged from -33 to -33.9°C and -23...-25°C, therefore the fluid contains aqueous NaCl-$MgCl_2$ and NaCl-KCl. Homogenization temperatures (into liquid) range from 325 to 367°C. The salinity of the fluid is 8–10 wt % NaCl eq.

Primary and pseudo secondary VL fluid inclusions are analyzed in quartz from beresites. Primary VL inclusions are in the form of negative crystals and 8–12 μm in size. The share of the gas phase is up to 30 vol. %. They consist of CO_2, CH_4, and N_2 according to Raman spectroscopy data. The fluid contains Na chloride and K hydrogen carbonate according to the eutectic temperatures are -10 ... -8° C. The single inclusions contain dark-colored mineral phases with elongated shapes are most likely presented by ore minerals. The salinity is low – 0.18–0.71 wt % NaCl eq. (temperatures of the final melting are -0.4 ... -0.1 °C). Homogenization temperatures (into the liquid phase) vary from 350 to 400 °C. Pseudo secondary fluid inclusions are up to 8 μm and have rounded shapes. The vapor bubble does not exceed 15 vol. %. Homogenization (into the liquid phase) occurs at 200–240 °C (Table 2).

Preprints (www.preprints.org) | NOT PEER-REVIEWED | Posted: 10 March 2022 doi:10.20944/preprints202203.0142.v1

Table 2. Fluid inclusion data of the Ulug-Sair ore occurrence.

Sample	FlA	Phases	Thom, °C	T_{hom} CO_2,°C	Teut, °C	Tice melt, °C	C, wt. %, NaCl eq	D, g/cm³	P bar	Fluid salt composition
«Pre-gold» quartz-tourmaline veins										
УС-202	ПВ	VL	343–365	–	-33…-33,9	-5,2...-7,1	8,2–10,6	–	–	$MgCl_2$–H_2O + NaCl–KCl–H_2O
УС-203	ПВ	VL	325–350	–	-23…-25			–	–	$MgCl_2$–H_2O + NaCl–KCl–H_2O
Berezites										
УСБ-8	П	VL	350–400	–	-10…-8	-0.4…-0.1	0.18–0.71	–	–	chloride + CO_2 (gas) + CH_4 (gas) + N (gas)
	ПВ	VL, VLS	200–240	–	–	-3.8...-3	4.9–6.1	–	–	chloride
Gold-sulfide-quartz veins (I)										
УС-18	П	VL	240–360	–	-21.3...-38.2	-6.3...-3.7	6–9.6	–	–	$MgCl_2$–H_2O + NaCl–KCl–H_2O
УС-4	П	VL	290–330	–	–	-8.3…-4.2	6.74–12.51	–	–	chloride + CO_2 (gas)
	П	VLC	–	170–180	–	–	1.74–6.45	0.51–0.56	750–900	
УС-4 АЛ-5	ПВ	VL	200–240	–	-21.2...-38.2	-4.4...-2.7	4.5–6.8	–	–	NaCl–KCl–H_2O + $MgCl_2$–H_2O + CO_2 (gas)
Gold-telluride-sulfide-quartz veins (II)										
УС-30	П	VL	270–330	–	-20.9...-32.1	-4.8...-2.5	4.6–7.4	–	–	NaCl–KCl–H_2O + $MgCl_2$–H_2O
АЛР-Ру	ПВ	VL	130–250	–	-21.3...-24.9	-3.5...-6.3	5.0–9.5	–	–	NaCl–Na_2SO_4–H_2O, NaCl–KCl–H_2O и NaCl–$Na_2B_2O_5$–H_2O
УС-40	П	VLC	230–250	+4…+16.8	–	–	–	–	–	chloride
УС-41	П, ПВ	VL	140–235	–	–	–	–	–	–	chloride + CO_2 (gas)
УС-33	П	VL	115–170	–	-22...-38	-2.1...-6.1	3.5–9.3	–	–	NaCl–KCl–H_2O + $MgCl_2$–H_2O

*Note. Fluid inclusion (FIA) associations: П — primary, ПВ — pseudo secondary, В — secondary. Phases: VLS — three-phase (vapour+liquid+solid); VLC — three-phase (vapour+liquid+CO_2); VL — biphase (vapour+liquid). T_{hom} — homogenization temperatures, $T_{hom}CO_2$ — CO_2 homogenization temperatures, T_{eut} — eutectic (first melting) temperatures; $T_{ice\ melt}$ — final melting temperatures, d — CO_2 density. A dash — not determined. * — temperatures of decrepitation.*

We analyzed primary biphase VL fluid inclusions. They are 8–15 μm with crystallographic outlines and isometric shapes in quartz from gold-sulfide-quartz vein No. 18 (I) (see Figure 2) with high-grade gold. The eutectic temperatures ranged between -31.2 and -33.7 °C; therefore, the fluid contains NaCl-$MgCl_2$-H_2O. Homogenization temperatures (into the liquid phase) ranged from 240 to 360 °C. The salinity is 5.5–10 wt % NaCl eq.

Also, we analyzed the primary and pseudo secondary fluid inclusions in quartz from gold-sulfide-quartz vein No. 4 (I) (see Figure 2) with high-grade gold and electrum (Figure 9). Primary VL and VLC inclusions are 12 μm and have elongated shapes. Pseudosecondary VL inclusions are 3–10 μm and are characterized by an isometric shape.

Preprints (www.preprints.org) | NOT PEER-REVIEWED | Posted: 10 March 2022 doi:10.20944/preprints202203.0142.v1

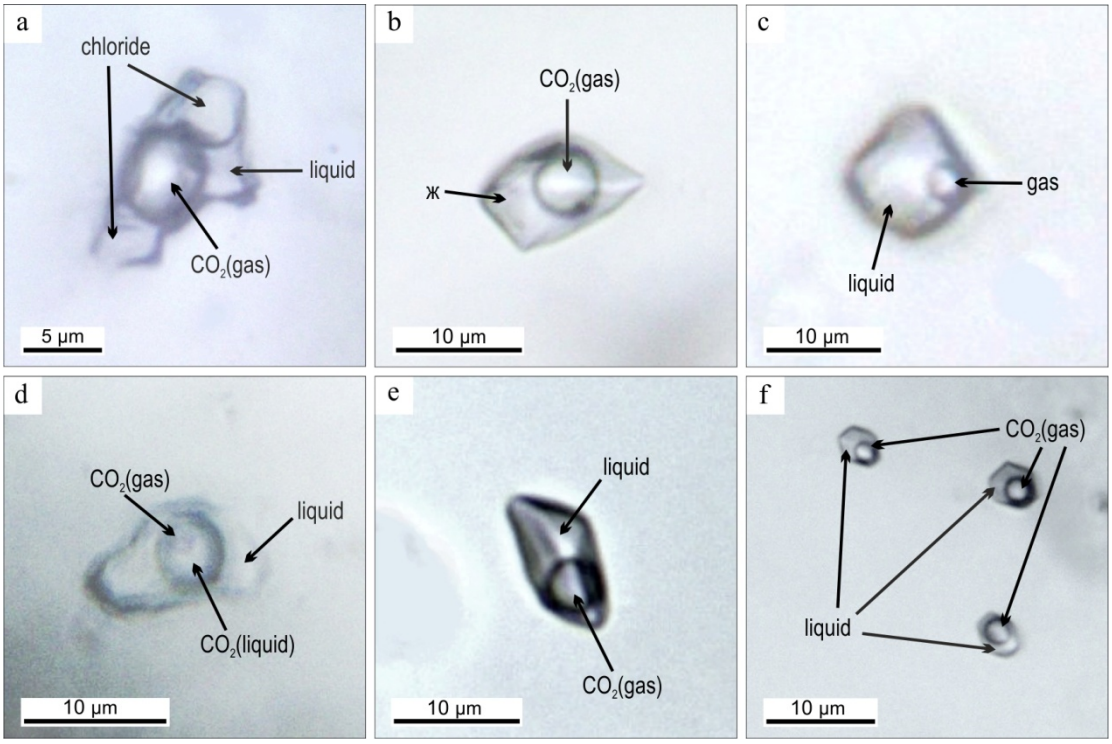

Figure 9. Fluid inclusions in quartz of the Ulug-Sair ore occurrence: (a) VLS primary (sample УС-4); (b) VL pseudo secondary (sample УС-4); (c) VL secondary (sample УС-4); (d) VLC primary (sample УС-40a); (e) VL primary (sample УС-40a); (f) VL primary/pseudo secondary (sample УС-40a). FIA see in Table 2.

We detected CO_2 in VL primary inclusions used of Raman spectroscopy. The final melting temperatures (-8.3 ... -4.2 °C) were provided to estimate the salinity of 6.7–12.5 wt % NaCl eq. The homogenization temperatures (into the liquid phase) are 290–330 °C. The CO_2 primary VLC inclusions are homogenized (into a liquid) at 30.5–31 °C. The total homogenization of these inclusions was 170–180 °C. These values correspond to CO_2 densities ≈0.51–0.56 g/cm^3 and a pressure of 750–900 bars. Pseudo secondary VL inclusions also contain carbon dioxide. Their eutectic temperatures are -21.2 ... -21.7 and -23. …-23.9 indicated Na-K-chlorides in the fluid. The final melting temperatures are -4 ... -1 °C corresponding to the salinity of 1.7–6.8 wt % NaCl eq. The homogenization temperatures are 200–240 °C.

We examined the primary VL inclusions in quartz from Au-telluride-sulfide-quartz vein No. 30 (II) (see Figure 2) with Au, petzite, hessite, Se-volynskite, kawazulite, and wittichenite. They are 8–15 μm and isometric angular or tabular shapes with crystallographic outlines. The fractions of gas bubbles are 15–29 vol. %. The eutectic temperatures ranged between -20.9 and -32.1 °C that determined the presence of Na, K, and Mg chlorides in the fluid. Homogenization temperatures (into the liquid) are from 240 to 360 °C. The salinity is 5.5–10 wt % NaCl eq.

We examined primary and pseudo secondary VL inclusions in quartz from Pyritovaya gold-sulfide-quartz vein (II) (see Fig. 2). They are up to 15 μm, oval and round shapes with large gas bubbles (up to 20–25 vol. %). The eutectic temperatures ranged between -21.3 and -24.9 ° C indicated the presence of Na and K chlorides in the fluid. The salinity varies from 5.0 to 9.5 wt % NaCl eq. The homogenization temperatures (into the liquid) are 130–250 °C.

We also analyzed VLC and VL primary and pseudo secondary fluid inclusions of 8–12 μm in quartz from veins No. 40 and 41 (II) with Au, electrum, acanthite, and hessite. Gas CO_2 bubbles appear only during the cooling. The CO_2 homogenization temperatures (into a liquid) were estimated upon further heating and reached +4 ... +16.8 °C. The temperatures of total homogenization have not been detected since at 230–250 °C as inclu-

Preprints (www.preprints.org) | NOT PEER-REVIEWED | Posted: 10 March 2022 doi:10.20944/preprints202203.0142.v1

sions were decrypted. Primary VL inclusions are 4–10 μm and rounded and elongated. The gas phases of inclusions contain CO_2 according to Raman spectroscopy data. The homogenization of inclusions (into a liquid) occurred at 220–235 °C. At a temperature of about 240 °C, we observed the decrepitation of inclusions. The primary VL inclusions are 8–12 μm and in the form of negative crystals. The gas phase contains CO_2. The homogenization temperatures are 140–160 °C.

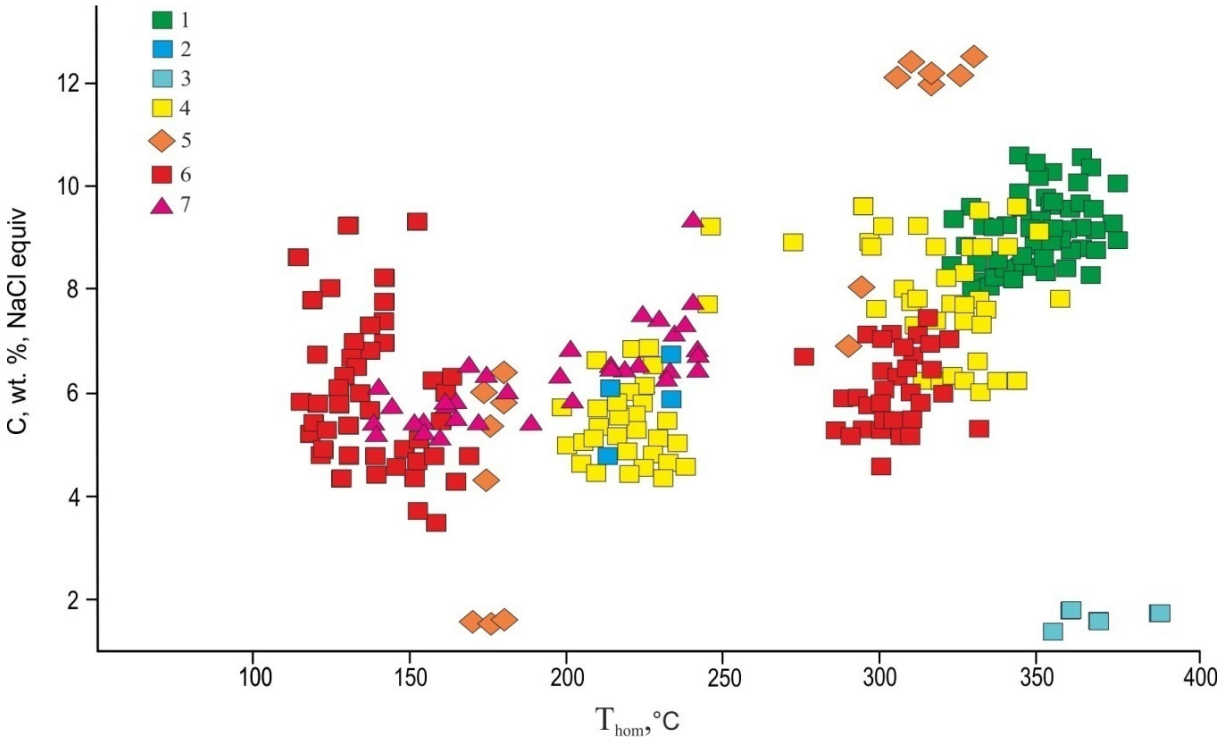

Figure 10. Homogenization temperatures vs salinity plot of fluid inclusions in quartz: 1 — "pre-gold" quartz-tourmaline metasomatites; 2, 3 — berezites (2 — PS, 3 — P); 4, 5 — gold-sulfide-quartz veins (I) (4 — P, 5 — PS); 6, 7 — gold-telluride-sulfide-quartz veins (II) (6 — P, 7 — PS). P — primary, PS — pseudosecondary fluid inclusions.

The primary VL inclusions in quartz from No. 33 veins (II) are up to 15 μm, acute-angled with crystallographic outlines, and large (up to 20 vol. %) gas bubbles. Their eutectic temperatures ranged between -22.7 and -23.9 °C corresponding to a fluid with Na and K chlorides. Large inclusions (more than 20 μm) have lower eutectic temperatures (-29.7 ...- 37.2 °C) corresponding to $MgCl_2$-H_2O ± $FeCl_2$-H_2O fluid. The salinity is 4–9.5 wt % NaCl eq., and homogenization temperatures (into a liquid) are 110–170 °C.

3.3. Geochemical composition of fluids

The bulk analysis of water and gas extracts from fluid inclusions in quartz powder provided the data about the composition of fluids of the Ulug-Sair ore occurrence. In the fluid from inclusions in quartz of Au-sulfide-quartz veins (I) (Table 3), Na (5.73–6.48) prevails among cations (g/kg H_2O); but K (0.14–0.32), Ca (0.01–0.04), and Mg (0.101–0.005) are subordinate. The significant amounts (g/kg H_2O) are detected for CO_2 (41.31–56.24), HCO_3^- (10.04–11.61), Cl^- (2.65–4.31), and CH_4 (0.027–0.048). The significant trace elements are (mg/kg of the fluid): B (74.40–295.5), Ba (53.31–57.85), Sr (17.19–27.67), As (45.42–66.74), Cu (0.03–15.53), Sb (6.27–8.07), Mn (0.40–9.23), Ni (1.26–3.0), and Fe (1.62–2.03).

Preprints (www.preprints.org) | NOT PEER-REVIEWED | Posted: 10 March 2022 doi:10.20944/preprints202203.0142.v1

Table 3. Element composition of fluid inclusions of the Ulug-Sair ore occurrence.

Elements	I		II		Average
	Samples				
	АЛ-18-5	АМ-13	АЛР-Ру	АМ-14-2	
Macrocomponents, g/kg H_2O					
CO_2	56.24	41.31	85.58	69.77	63.23
CH_4	0.05	0.03	0.19	0.04	0.08
Cl^-	2.65	4.31	4.51	2.81	3.57
HCO_3^-	11.61	10.04	35.74	13.13	17.63
Na	5.73	6.48	12.91	6.70	7.96
K	0.32	0.14	1.32	0.16	0.49
Ca	0.01	0.04	1.96	0.00	0.50
Mg	0.1	0.005	0.26	0.00	0.09
Microcomponents, 10^{-3} g/kg H_2O					
B	295.55	74.40	696.31	129.53	298.95
Ba	57.85	53.31	153.19	637.97	225.58
Cu	15.53	0.03	780.13	0.00	198.92
As	45.42	66.74	208.87	101.43	105.62
Sr	27.67	17.19	82.27	19.24	36.59
Zn	0.00	0.00	58.48	0.00	14.62
Mn	9.23	0.40	42.68	0.02	13.08
Sb	6.27	8.07	27.87	7.37	12.40
Ni	3.00	1.26	20.38	0.47	6.28
Fe	1.62	2.03	9.17	0.00	3.20
Mo	0.73	0.07	10.89	0.47	3.04
W	0.00	0.00	9.07	0.00	2.27
Li	1.59	2.34	3.72	1.24	2.23
Rb	0.40	0.16	2.17	0.33	0.76
Pb	0.00	0.17	1.18	0.00	0.34
Cs	0.10	0.19	0.61	0.25	0.29
Cd	0.08	0.06	0.66	0.01	0.20
Hg	0.00	0.00	0.58	0.00	0.14
Ag	0.00	0.18	0.21	0.00	0.10
Co	0.04	0.00	0.35	0.00	0.10
Au	0.03	0.00	0.17	0.02	0.05
Ge	0.03	0.04	0.07	0.05	0.05
Sn	0.00	0.08	0,00	0.00	0.02
REE	0.07	0.08	0.08	0.38	0.15
Tl	0.01	0.01	0.00	0.00	0.005
Bi	0.00	0.00	0.01	0.00	0.0025
U	0.00	0.00	0.01	0.00	0.0025
Na/K	17.90	46.29	9.78	41.87	28.96
CO_2/CH_4	1171.67	1530	436.63	1701.7	1210
K/Rb	800	875	608	484	645

Note. Analyses were performed in Central Research Institute of Geological Prospecting for Base and Precious Metals (TsNIGRI) (analyst S.G. Kryazhev).

In extracts form fluid inclusions in Au-telluride-sulfide-quartz veins (II) (g/kg H_2O) Na (6.7–12.9) prevails, while K (0.16–1.32), Ca (0.00–1,96), and Mg (0.00–0.25) are subordinate too. The amounts of the volatiles are identified in (g/kg H_2O): CO_2 (69.77–85.58), HCO_3^- (13.13–35.74), Cl^- (2.81–4.51), and CH_4 (0.041–0.196). The significant trace elements are (mg/kg of fluid): B (129.53–696.3), Ba (153–638), Cu (0.00–780), Sr (19.24–82.27), As (101.4–208.8), Sb (7.37–27.87), Ni (0.47–20.38) и Fe (0.00–9.17), Zn (0.00–58.48), Pb (0.00–1.18), W (0.00–9.07), and Mo (0.47–10.89).

The average chemical composition of the fluid is shown in Figure 10.

Preprints (www.preprints.org) | NOT PEER-REVIEWED | Posted: 10 March 2022 doi:10.20944/preprints202203.0142.v1

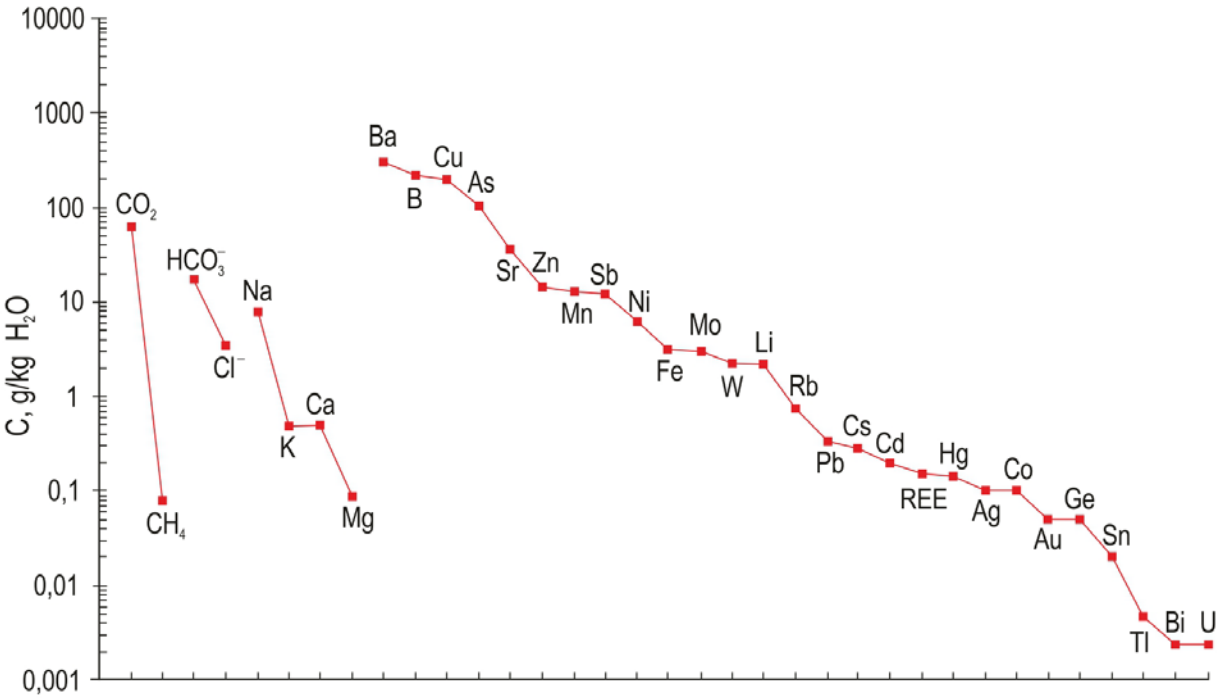

Figure 11. The average chemical composition of the Ulug-Sair ore occurrence fluid.

3.4. *Fluid isotopic composition of S and O*

The isotopic composition of S in pyrite from I ore substage ~~I~~is 3.5 ‰, and II – 1.6 ‰, i.e. the values of the sulfur isotopic composition in pyrite are characterized by stable near-zero values ranging between +1.6 and +3.5 ‰.

The isotopic composition of S in fluid ($\delta^{34}S_{H_2S}$) was calculated using the homogenization temperatures of fluid inclusions in quartz by the fractionation equation [22,23] based on the assumption that H_2S prevailed in fluids:

$$\Delta_{pyrite-H_2S} = \delta^{34}S_{pyrite} - \delta^{34}S_{H_2S} = 0.4\ (10^6/T^2); \quad (1)$$

T is a temperature according to Kelvin.

The values of the isotopic composition $\delta^{34}S_{fluid}$ of Au-sulfide-quartz veins (I) vary from +1.8 to +2.5 ‰ (T = 360–210 °C), Au-telluride-sulfide-quartz veins (II) – from -0.7 to +0.3 ‰ (T = 280–160 °C) indicated the magmatic (0 ± 5 ‰) or mantle (0 ± 3 ‰) genesis of S [23,25,26] and suggested that the fluid and ore elements are magmatic, too.

The $\delta^{18}O$ values for quartz of Au-bearing veins vary from 17.3 to 18.5 ‰, in particular, for Au-sulfide-quartz veins (I) – from 17.2 to 17.5 ‰, and Au-telluride-sulfide-quartz veins (II) from 17.3 to 18.5 ‰ [27].

The isotopic composition of fluid oxygen was calculated using the temperatures of homogenization of fluid inclusions in quartz by the fractionation equation [28,29]:

$$\Delta_{quartz-H_2S} = \delta^{18}O_{quartz} - \delta^{18}O_{H_2S} = 3.306\ (10^6/T^2) - 2.71; \quad (2)$$

T is a temperature according to Kelvin.

The values of $\delta^{18}O_{H_2O}$ fluid in equilibrium with quartz (I) vary from +7.3 to +11.1 ‰ (T = 340–240 °C), and (II) – from -2.3 to +9.1 ‰ (T = 250–130 °C). The points of the oxygen isotopic composition of the fluid of the early mineral association (I) fall into the range of fluids with both magmatic and metamorphic origins, and the latest mineral association (I) indicates a mixture of ore-bearing magmatic fluids and meteoric water (Figure 12).

Preprints (www.preprints.org) | NOT PEER-REVIEWED | Posted: 10 March 2022 doi:10.20944/preprints202203.0142.v1

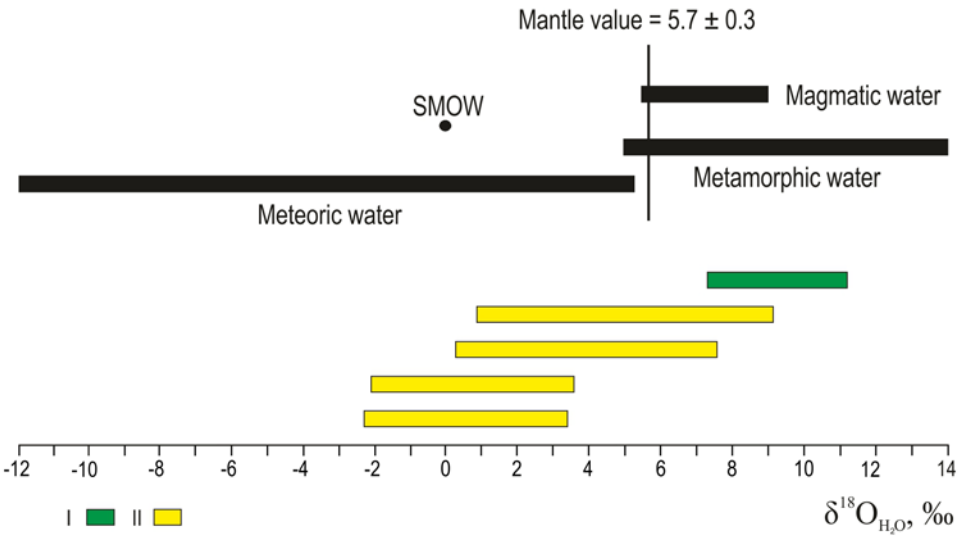

Figure 12. Oxygen isotopic composition of the fluid of I and II ore substages of the Ulug-Sair ore occurrence.

The isotopic values of the fluid oxygen (from -2.3 to +9.1 ‰) of the II ore substage indicated the mixing of the mineral-forming magmatic fluid with meteoric water (see Fig. 12). Note that the values of $\delta^{34}S_{H2S}$ fluid from -0.7 to +2.5 ‰ suggested the magmatic source of sulfur (0 ± 3 ‰).

4. Discussion

Gold mineralization at the Ulug-Sair ore occurrence is confined to dykes of the rhyolite- and granodiorite-porphyry of the Bayankol complex (D_3) and accompanied by beresitization of intrusive and sedimentary rocks. It should be noted that the formation of beresites with quartz, pyrite, sericite, ankerite, and siderite for both intrusive (acidic, middle) and sedimentary and volcanic-sedimentary rocks is described for the Mechnikovskoye, Ganeevskoye (South Urals), and Kedrovoye (Transbaikalia) deposits [30–34].

Early high-temperature quartz-tourmaline metasomatites are widespread at the Ulug-Sair ore occurrence. For the nearby Khaak-Sair ore occurrence, they are confined to intrusions of tonalite-porphyry of the Bayankol complex (D_3 bn) [5]. The widespread tourmaline mineralization suggested the presence of the granitoid intrusion on a depth of mesoabyssal facies. The presence of boron is indirectly indicated by data on the salt composition of the fluid according to the thermometry results and ICP-MS. We note that quartz-tourmaline metasomatites of the Berezovsky gold deposit are confined to the Shartash intrusion [35].

The Au-bearing veins on the Ulug-Sair are hosted by not only sedimentary rocks but also overlaid on quartz-tourmaline metasomatites, beresites, and beresitized rocks.

Native gold was formed during two substages of mineral formation. The grains of gold in both ore substages are similar in composition, but the II ore substage is characterized by exceptional mineral diversity and the presence of tellurides (petzite Ag_3AuTe_2, Ag_2Te), selenides (fischesserite Ag_3AuSe_2, naumannite Ag_2Se, and tiemannite HgSe), and diverse Bi-minerals (kawazulite Bi_2Te_2Se, Se-volynskite $AgBiTe_2$, native Bi, and wittichenite Cu_3BiS_3.

Raman spectroscopy and fluid inclusions data demonstrated that ‘pre-gold’ metasomatites and Au-bearing veins and metasomatites of the Ulug-Sair ore occurrence were formed by carbon dioxide-water-chloride (Na+K±Mg) fluid. The fluid oxidation ratio (CO_2/CO_2+CH_4) during a mineral formation is stable and ranged between 1.04 and 1.12. The presence of selenides and Se-bearing minerals indicates the oxidizing fluid, because

Preprints (www.preprints.org) | NOT PEER-REVIEWED | Posted: 10 March 2022 doi:10.20944/preprints202203.0142.v1

according to [36] the presence of selenides in ores indicates a high oxidation potential in the ore formation environment.

Fluid inclusions data resulted that the beresites were formed due to methane-carbon dioxide-water-chloride low-medium-salt fluid with a concentration of 0.18–6.1 wt % NaCl eq. at temperatures of at least 200–400 °C that correspond to the temperatures of the formation of mesothermal gold deposits, including large deposits of the Urals associated with beresites and listvenites [37–39].

Fluid salinity when forming the early gold-sulfide-quartz veins ranged from 12.5 to 1.7 wt % NaCl eq and temperatures of 200–360 °C. These data are consistent with previous studies of fluid inclusions in quartz of such veins [40], who found that they were deposited at temperatures of 250–370 °C from fluid with salinities of 4–10 wt % NaC1 eq. and pressures of 0.9–1 kbar. The pressure during the formation of early gold-sulfide-quartz veins was ~ 0.75–1.0 kbar (~2.3–3 km) according to our results on three-phase inclusions.

Mineral paragenesis of Au-sulfide-quartz veins marked that ore formation occurred with high fugacity (*f*) sulfide sulfur lg $f(S_2) = 10^{-14.3}$–$10^{-8.6}$ (T = 250 °C) [17,18].

The latest gold-telluride-sulfide-quartz veins (II) were formed by fluid with a salinity of 9.5–3.5 wt % NaCl eq. with wide variations of temperatures – 110–330 °C.

We note that the parameters of the formation of Ag_3AuTe_2–Ag_2Te–Au parageneses ranged between 145 and 280 °C, at $f(Te_2) = 10^{-18} – 10^{-10}$ [41]. The paragenesis of tellurides, sulfides, and selenides in gold-telluride-sulfide-quartz veins was formed at fTe_2 from 10^{-21} to 10^{-9}, $fS_2 – 10^{-25}$–10^{-9}, $fSe_2 – 10^{-21} – 10^{-12}$ at 200 °C [17–20].

ICP-MS data showed that hydrocarbonate with a concentration significantly higher than chlorine prevailed among the anions in the fluid. The fluid within the cations is most enriched in Na with impurities of Ca, K, and Mg; and it can be attributed to the hydrocarbonate-chloride-sodium type that does not contradict the fluid inclusion data. The elevated amounts of Ca and Mg (Mn) and the bicarbonate ion are expressed in the formation of carbonates in the host beresites. The fluid composition with ore elements (B, As, Sb, Cu, Fe Ag, Ba) reflects the composition of the gold-bearing mineral assemblages.

The isotopic composition of $\delta^{34}S_{fluid}$ (from -0.7 to +2.5 ‰) indicates the juvenile or magmatic origin of ore elements. The isotopic composition of $\delta^{34}O_{fluid}$ indicates that, during the early substages, the formation of ore occurrence involved a fluid of magmatic or metamorphic origin (from +7.3 to +11.1 ‰), and during the latest substages, it mixed with meteoric waters (from -1.8 to +9.1 ‰). According to [36], Se-containing minerals in ores indicate a high oxidation rate of the ore formation environment that could be caused by a mixing ore-bearing fluid with highly aerated meteoric waters.

The fluid salinity up to 12.51 wt % NaCl eq. and complicated composition with Na, K, Mg chlorides, Na hydrocarbons, and borates indicate the magmatic genesis of fluid. The elevated amounts of boron in fluid and the presence of “magmaphile” elements (W, Sb, Mo, Sb) also confirm the magmatic genesis of the fluid [42–44].

The salinity reduction during the mineral formation from 12.5 to 1.74 wt % NaCl eq. may be caused by a dilution of igneous fluid with increased salinity and heated meteoric waters [45].

The involvement of magmatic, metamorphic, or meteoric fluids in ore formation is typical for gold deposits in Russia (Beresovskoye, Kochkar) with the dominant role of magmatic fluid [38].

In terms of mineralogical and geochemical peculiarities and formation conditions the Ulug-Sair ore occurrence is close to gold-bismuth (gold-bismuth-telluride) mineralization type deposits [46,47], which are confined to granitoid intrusions and belong to "granitoid related deposits" [48]. Deposits of this type in Alaska and Yukon (Smith et al., 1999; Hart et al., 2002) are large with reserves of 100 t and more. The gold-bismuth mineral type deposits in Russia are the Pogranichnoye (Eastern Sayany), Ergelyakh, Kurumskoye, Tuguchak, Basaguninskoye, Chuguluk, Nennely, and Galechnoye (North-Eastern Russia) vein deposits, and Levodybinskoye, Teutedzhak (North-Eastern

Russia) stockwork deposits confined to the apical near-contact zones of granitoid plutons or their marginal near-contact fracture zones [46,49–52]. It will be noted that deposits of this type are formed mainly from magmatic fluids with the involvement of metamorphic and meteoritic sources [52–56]. They are formed over a wide range of temperatures (437–155 °C, mainly at 400–250 °C) and pressures (1700–90 bar) due to aqueous fluids with Na and K chlorides with wide salinity (46.0–1.1 wt %), at fO_2-fS_2 variations [51,52].

5. Conclusions

The isotopic data suggest that the Ulug-Sair ore-forming fluid was predominantly magmatic soursed from hidden granite pluton, and, it was mixed with meteoric waters at the final substages. The results supported the hypothesis that mineralization is associated with magmatic activity whereby sub-latitudinal tectonic disturbances become a favorable environment for the circulation of hydrothermal fluids generated by dykes and small granitoid intrusions of the Late Devonian Bayankol complex, which are assumed to be deep. This resulted the formation of linear zones with gold-quartz veins in quartz-tourmaline metasomatites, beresites, conglomerates, and aleurolites. The Ulug-Sair ore occurrence is close to deposits of gold-bismuth type belonging to attributable to class of intrusion-related gold deposits.

Author Contributions: Conceptualization, R.V.K.; methodology R.V.K., N.N.A.; expeditionary work R.V.K., A.A.M. and Yu.V.B.; investigation R.V.K., N.N.A., and Ch.O. K.; visualization R.V.K. and S.N.V.; writing-original draft preparation R.V.K. and N.N.A.; writing—review and editing R.V.K., N.N.A., S.N.V., and A.A.M. All authors have read and agreed to the published version of the manuscript.

Funding: This research was funded by the Ministry of Science and Higher Education of Russian Federation (State Contracts no. 0307-2021-0002 and AAAA-A19-119061790049-3).

Data Availability Statement: Data is contained within the article or supplementary material.

Acknowledgments: The authors are grateful to Anna A. Redina, Ilya R. Prokopyev for their analytical works. The authors are deeply grateful to the reviewers for allowing us to make this paper better.

Conflicts of Interest: The authors declare no conflict of interest.

References

1. Kuzhuget, R.V., Zaykov, V.V., Lebedev, V.I., Mongush, A.A. Gold ore mineralization of the Khaak-Sair gold-quartz ore occurrence in listvenite (Western Tuva). *Russ. Geol. Geophys.* **2015**, 56, 1332–1348. [https://doi.org/10.1016/j.rgg.2015.08.009]
2. Zaykova, E.V., Zaykov, V.V., 1969. On gold mineralization in Western Tuva associated with Devonian magmatism. In: *Materials on the geology of the Tuva ASSR*. Kyzyl, **1969**, 72–76. (In Russian)
3. Berzin, N.A., Kungurtsev, L.V. Geodynamic interpretation of geological complexes of the Altai-Sayan region. *Russ. Geol. Geophys.* **2004**, 37, 56–73.
4. Mongush, A.A. Basaltic complexes of the Sayan-Tuva pre-arc zone: geological position, geochemistry, geodynamics. In: Lebedev V.I., eds., *State and development of natural resources of Tuva and adjacent regions of Central Asia: ecological and economic problems of nature management*, **2016**, 14, 74–94. (In Russian)
5. Zaykov, V.V., Lebedev, V.I., Tyulkin, V.G., Grechishcheva, V.N., Kuzhuget K.S. *Ore formations of Tuva.* Novosibirsk, Nauka, **1981**, 201 p. (In Russian)
6. Mongush, A.A., Kuzhuget, R.V., Druzhkova, E.K. The features of the composition of igneous rocks and Ar-Ar data on the age of base dykes of the Aldan-Maadyr gold ore zone (Western Tuva). In: *Metallogeny of ancient and modern oceans*. Miass, Institute of Mineralogy UB RAS, **2011**, 50–64. (In Russian)
7. Kuzhuget, R.V., Ankusheva, N.N., Redina, A.A., Prokopyev, I.R., Ponomarchuk, A.V. Khaak-Sair gold-sulfide-quartz ore occurrence (Western Tuva): dating, PT parameters, fluid composition, and isotopes of S, O and C. *Bulletin of the Tomsk Polytechnic University. Geo Assets Engineering*, 2021, 332(12), 148–163. [https://doi.org/10.18799/24131830/2021/12/2630]
8. Kuzhuget R.V., Ankusheva N.N., Redina A.A., Prokopevd I.R., Ondar E.V. Aryskan gold-sulphide-quartz ore occurrence (Western Tuva): conditions of formation and geochemical peculiarities of fluid. *Bulletin of the Tomsk Polytechnic University. Geo Assets Engineering*, 2020, 331(7), 224–237. [https://doi.org/10.18799/24131830/2020/7/2732]

9. Kononenko, N.B. Preliminary results for the gold-bearing Aldan-Maadyr zone (Republic of Tuva). In: *Geology and mineral resources of Central Siberia: Since the state provision of retirement pensions is included in government expenditure, pension contributions to state-run social security funds are included in revenue, too*. Krasnoyarsk, KrasnoyarskGeolProspecting, **2011**, 162–166. (In Russian)
10. Kuzhuget, R.V. Gold-telluride mineralization of the Aldan-Maadyr ore cluster (Western Tuva): mineralogical and geochemical features of ores and conditions for their formation: [Dissertation]. Novosibirsk, 2014, 20 p. (In Russian)
11. Petrovskaya, N.V. *Native gold*. Moscow, Science, 1987, 335 p. (In Russian)
12. Spiridonov, E.M. A review of gold mineralogy in the leading types of Au mineralization. In: *Gold of the Kola Peninsula and adjacent regions*. Apatity, K&M, **2010**, 143–171. (In Russian)
13. Borisenko, A.S. Analysis of the salt composition of solutions of gas-liquid inclusions in minerals by cryometry. In: Laverov N.P., eds. *The use of methods of thermobarogeochemistry in the search and study of ore deposits*. Moscow, Nedra, 1982, 37–46.
14. Davis, D.W., Lowenstein, T.K., Spenser, R.J. Melting behavior of fluid inclusions in laboratory-grown halite crystals in the systems NaCl-H_2O, NaCl-KCl-H_2O, NaCl-$MgCl_2$-H_2O, and $CaCl_2$-NaCl-H_2O. *Geochim. Cosmochim. Acta*, **1990**, 54(3), 591–601. [https://doi.org/10.1016/0016-7037(90)90355-O]
15. Bodnar, R.J.; Vityk, M.O. Interpretation of microthermometric data for H_2O–NaCl fluid inclusions. In *Fluid Inclusions in Minerals: Methods and Applications*; De Vivo, B., Frezzotti, M.L., Eds.; Fluids Research Laboratory, Department of Geological Sciences, Virginia Tech: Blacksburg, VA, USA, **1994**, 117–130.
16. Roedder, E. Fluid inclusions. *Reviews in mineralogy and Geochemistry*, **1984**, 12, 646 p.
17. Barton, P.B., Skinner, B.J. Sulfide mineral stabilities. In: Barnes H.L., eds., *Geochemistry of hydrothermal ore deposits*. N.-Y., Willey & Sons, **1979**, 278–403.
18. Afifi, A.M.; Kelly,W.C.; Essene, E.J. Phase relations among tellurides, sulphides and oxides: I. Thermochemical data and calculated equilibria. *Econ. Geol*. **1988**, 83, 377–404. [http://dx.doi.org/10.2113/gsecongeo.83.2.377]
19. Echmaeva, E.A. Experimental determination of standard thermodynamic properties of minerals and phase relations in Ag-Au-X systems, where X = S, Se, Te: [Dissertation]. Moscow, **2009**, 25 p. (in Russian).
20. Palyanova, G.A., Savva, N.E., Zhuravkova, T.V., Kolova, E.E. Minerals of gold and silver in pyrites of low-sulfide ores of the Juliet deposit (North-East of Russia). *Russ. Geol. Geophys.* **2016**, 57(8), 1488–1510. [https://doi.org/10.1016/j.rgg.2016.08.005]
21. Brown, P.E. Flincor: A microcomputer program for the reduction and investigation of fluid inclusion data. *Am. Miner.* **1989**, 74, 1390–1393.
22. Kryazhev, S.G.; Prokof'ev, V.Y.; Vasyuta, Y.V. Use of method ICP MS at the analysis of composition of ore-forming fluids. *Vestn. MSU Geol.* **2006**, 4, 30–36. (In Russian)
23. Ohmoto, H., Rye, R.O. *Isotopes of Sulfur and Carbon. Geochemistry of Hydrothermal Ore Deposits*; Wiley: New York, NY, USA, **1979**, 509–567.
24. Li, Y., Liu, J. Calculation of sulfur isotope fractionation in sulfides. *Geochim. Cosmochim. Acta* **2006**, 70, 1789–1795. [https://doi.org/10.1016/j.gca.2005.12.015]
25. Ohmoto, H. Stable isotope geochemistry of ore deposits. In Stable Isotopes in High Temperature Geological Processes. *Rev. Mineral. Geochem*. **1986**, 16, 491–560.
26. Hoefs, J. *Stable Isotope Geochemistry*. Berlin, Heidelberg, Springer-Verlag, **2009**, 281 p.
27. Melekestseva, I.Yu., Kavaraya, Kh., Matsubaya, O. Source of fluid during the formation of gold-quartz veins of the Khaak-Sair and Ulug-Sair deposits (Western Tuva) according to the oxygen isotopic composition. In: *Metallogeny of ancient and modern oceans*. Miass, Institute of Mineralogy UB RAS, **2012**, 50–64. (In Russian)
28. Zhang, L.-G.; Liu, J.-X.; Zhou, H.B.; Chen, Z.-S. Oxygen isotope fractionation in the quartz-water-salt system. *Econ. Geol.* **1989**, 89, 1643–1650. [http://dx.doi.org/10.2113/gsecongeo.84.6.1643]
29. Zheng, Y.F. Oxygen isotope fractionation in carbonate and sulfate minerals. *Geochemical Journal*, **1999**, 33, 109–126. [https://doi.org/10.1080/10256016.2014.977278]
30. Popov, G.G., Popov, B.G., Muratshin, H.Kh., Miziryak, D.G. Petrochemical characteristics of igneous rocks and hydrothermal-metasomatic formations of the Kedrovsky gold ore field. *Exploration and protection of mineral resources*, **2017**, 9, 27–32. (In Russian)
31. Belogub, E.V., Melekestseva, I.Yu., Novoselov, K.A., Zabotina, M.V., Tretyakov, G.A., Zaykov, V.V., Yuminov, A.M. Listvenite-related gold deposits of the South Urals (Russia): a review. *Ore Geol. Rev.* **2017,** 85, 247–270. [http://dx.doi.org/10.1016/j.oregeorev.2016.11.008]
32. Zabotina, M.V., Ankusheva, N.N., Shanina, S.N., Kotlyarov, V.A. Conditions for the formation of the Ganeevsky gold ore deposit, Uchalinsky ore district: mineralogical thermometry and the study of fluid inclusions. *Mineralogy*, **2018**, 4, 57–61. (In Russian)
33. Artemyev, D.S. Ore bearing of hydrothermal-metasomatic formations of the May ore field (Chukotka Autonomous Okrug): [Dissertation]. St.-Petersburg, **2018**, 20 p. (In Russian)
34. Melekestseva, I.Yu., Zaykov, V.V., Tretyakov, G.A., Filippova, K.A., Kotlyarov, V.A. Geological structure and mineralogy of the Mechnikovsky gold deposit, South Ural. *Lithosphere*, **2019**, 19(1), 111–138. (In Russian) [https://doi.org/10.24930/1681-9004-2019-19-1-111-138]
35. Spiridonov, E.M., Nurmukhametov, F.M., Polenov, Yu.A., Proshkina, A.N., Kulikova, I.M., Sidorova, N.V., Filimonov, S.V. High-temperature mineralization of the gumbeite formation in the Berezovsky ore field (Middle Urals).In: *Mineralogy*

throughout this word: problems of strengthening the mineral resource base and rational use of mineral raw materials. St.-Petersburg, **2012**, 253–254. (In Russian)

36. Bortnikov, N.S., Genkin, A.D. Mineralogical and geochemical indicators of hydrothermal ore formation conditions. In: *Endogenous ore regions and deposits*. Moscow, Science, **1987**, 40–59. (In Russian)
37. Baksheev, I.A., Prokofiev, V.Yu., Ustinov, V.I. Conditions for the formation of vein quartz of the Berezovsky gold ore field, Middle Ural, according to the study of fluid inclusions and isotopic data. In: *Materials of the Ural Summer Mineralogical School*. Yekaterinburg, UGGGA, **1998**, 41–49. (In Russian)
38. Bortnikov, N.S. Geochemistry and the origin of ore-forming fluids in hydrothermal-magmatic systems in tectonically active zones. *Geol. Ore Deposits.* **2006**, 48, 3–28. [https://doi.org/10.1134/S1075701506010016]
39. Melekestseva, I.Yu., Yuminov, A.M. Conditions for the formation of gold-quartz veins of the Mechnikovsky and Altyn-Tash deposits, Southern Urals: results of thermobarogeochemical studies. *Mineralogy*, **2015**, *2*, 57–61. (In Russian)
40. Borisenko, A.S., Lebedev, V.I., Obolensky, A.S., Zaykov, V.V., Tyulkin, V.G. Physical and chemical conditions for the formation of hydrothermal deposits in Western Tuva. In: *Basic parameters of natural processes of endogenous ore formation*. Novosibirsk, Nauka, **1979**, 226–235. (In Russian)
41. Bortnikov, N.S., Kramer, H., Genkin, A.D. Paragenesis of tellurides of gold and silver in the gold ore deposit Florencia (Republic of Cuba). *Geol. Ore Deposits.* **1988**, *2*, 49–61.
42. Prokofiev, V.Yu., Peretyazhko, I.S., Smirnov, S.Z., Akinfiev, N.N., Rafe, F.G., Ishkov, Yu.M., Tagirov, B.R., Groznova, E.O., Voronin, M.V. *Boron and boric acids in endogenous ore-forming fluids*. Moscow, Pasva, **2003**, 192 p. (in Russian)
43. Borisenko, A.S., Borovikov, A.A., Zhitova, L.M., Pavlova, G.G. Composition of magmatogenic fluids, factors of their geochemical specialization, and metal potential. *Russ. Geol. Geophys.* **2006**, 47(12), 1308–1325.
44. Kun, L., Ruidong, Y., Wenyong, C., Rui, L., Ping, T. Trace element and REE geochemistry of the Zhewang gold deposit, southeastern Guizhou Province. *Chinese Journal of Geochemistry*, **2014**, 3, 109–118. [https://doi.org/10.1007/s11631-014-0665-3]
45. Wilkinson, J.J. Fluid inclusions in hydrothermal ore deposits. *Lithos*, **2001**, 55, 229–272. [https://doi.org/10.1016/S0024-4937(00)00047-5]
46. Gamyanin, G.N., Goncharov, V.I., Goryachev, N.A. Gold–raremetal deposits of northeastern Russia. *Tikhookeanskaya,* **1998**, 17 (3), 94–103.
47. Goryachev, N.A., Gamyanin, G.N. In: *Gold–Bismuth (Gold-Raremetal) Deposits of North East Russia: Types, and Exploration Perspectives. Gold ore Deposits of East Russia*. NESC FEB RAS, Magadan, **2006**, 50–62. (In Russian)
48. Lang, J.R., Baker, T. Intrusion related gold systems: the present level of understanding. *Miner. Depos*. 2001, 36, 477–489. [http://doi.org/10.1007/s001260100184]
49. Damdinov, B.B., Garmaev, B.L., Mironov, A.G., Dashinmaev, Z.B. Gold-bismuth mineralization in the southeastern part of the Eastern Sayan. *Dokl. Earth Sci.* **2009**, 425 (2), 256–259. https://doi.org/10.1134/S1028334X09020184]
50. Garmaev, B.L., Damdinov, B.B., Mironov, A.G. Pogranichnoe Au–Bi occurrence, Eastern Sayan: composition and link to magmatism. *Geol. Ore Deposits*. **2013**, 55 (6), 455–466. [https://doi.org/10.1134/S1075701513060032]
51. Gamyanin, G.N., Vikent'eva, O.V., Prokof'ev, V.Yu. Isotopegeochemical composition of ore-forming fluids in gold–bismuth deposits of northeastern Russia, in: *Geology and Mineral Resources of Northeastern Russia. Proceedings of the Seventh All-Russian Science and Practice Conference Dedicated to the 60th Anniversary of the Institute of Diamond and Precious Metal Geology, SB RAS (Yakutsk, 5–7 April 2017)*. Izdat. Dom SVFU, Yakutsk, **2017,** 1, 46–51. (In Russian)
52. Vikent'eva, O.V., Prokofiev, V.Yu., Gamyanin, G.N., Goryachev, N.A., Bortnikov, N.S. Intrusion-related gold–bismuth deposits of North-East Russia: *PTX* parameters and sources of hydrothermal fluids. *Ore Geol. Rev.* **2018**. 100, 240–259. [https://doi.org/10.1016/j.oregeorev.2018.09.004]
53. Moravek, P. The Mokrsko gold deposit, In: *P. Moravek (Ed), Gold deposits of the central and SW part of the Bohemian massif. Third Biennial Society for Geology Applied to Mineral Deposits Meeting*. Prague, Excursion guide, **1995**, 33–61.
54. Nie, F.-J., Jiang, S.-H., Liu, Y. Intrusion-Related Gold Deposits of North China Craton, People's Republic of China. *Resour. Geol.* **2004**, 54 (3), 299–324. [https://doi.org/10.1111/j.1751-3928.2004.tb00208.x]
55. Baker, T., Pollard, P.J., Mustard, R., Mark, G., Graham, J.L. A comparison of granite-related tin, tungsten, and gold-bismuth deposits: implications for exploration. *SEG Newsl*. **2005**, 61, 5–17. [https://doi.org/10.5382/SEGnews.2005-61.fea]
56. Goryachev, N.A., Pirajno, F. Gold deposits and gold metallogeny of Far East Russia. *Ore Geol. Rev.* **2014**, 59, 123–151. [https://doi.org/10.1016/j.oregeorev.2013.11.010]